Lithos 366–367 (2020) 105557

Contents lists available at ScienceDirect

Lithos

journal homepage: www.elsevier.com/locate/lithos

Research Article

Mesozoic crustal evolution of southern Tibet: Constraints from the early Jurassic igneous rocks in the Central Lhasa terrane

Xin Dong [a,b,*], Yaoling Niu [b], Zeming Zhang [a], Zuolin Tian [a], Zhenyu He [a]

[a] Key Laboratory of Deep-Earth Dynamics of Ministry of Natural Resources, Institute of Geology, Chinese Academy of Geological Sciences, Beijing 100037, China
[b] Department of Earth Sciences, Durham University, Durham DH1 3LE, UK

ARTICLE INFO

Article history:
Received 1 December 2019
Received in revised form 27 April 2020
Accepted 28 April 2020
Available online 04 May 2020

Keywords:
Cumulates
Granitoids
Assimilation–fractional crystallization
Mesozoic crustal evolution
Southern Tibet

ABSTRACT

Phanerozoic growth of continental crust on our planet is one of the important research themes in Earth Science. Here, we present the results of a systematic study of newly found and previously reported Mesozoic igneous rocks, including diorite cumulate, granodiorite cumulate, mafic magmatic enclaves (MME) and host granitoids in the central Lhasa terrane, southern Tibet. These igneous rocks give zircon U—Pb crystallization ages of 199–189 Ma. Based on constituent mineral and bulk-rock compositions, the cumulates are best understood as resulting from amphibole, plagioclase and titanite crystallization from a mafic andesitic magma. The host granitoids also show compositional systematics consistent with amphibole-plagioclase fractional crystallization from andesitic magma. The MMEs share many characteristics with their host granitoids in common, including identical crystallization age, similar mineralogy, mineral chemistry and zircon isotopic compositions, representing earlier cumulate derived from the same magmatic system as their host rocks. The magma parental to the studied Early Jurassic igneous rocks is best explained as resulting from partial melting of hydrated ocean crust together with varying continental material. The increasing zircon $\varepsilon_{Hf}(t)$ values of multiple plutons in the central Lhasa terrane with time during ~215–170 Ma indicate its gradual increase in mantle contribution. We present the Early Mesozoic crustal evolution in the Lhasa terrane.

1. Introduction

The Earth is the only planet in the solar system with oceans and continents with the continental crust standing above the sea level (e.g., Rudnick, 1995). The significance of the continental crust on which we live is self-evident, yet our knowledge remains limited on its origin and growth (Niu et al., 2013). Arc magmatism is widely accepted to be a fundamental process responsible for post-Archean continental crust growth (e.g., Rudnick and Gao, 2003; Taylor and McLennan, 1985). Therefore, understanding the origin and nature of arc crusts is critical for understanding the formation and evolution of continental crust (e.g., Jagoutz and Kelemen, 2015).

Unlike the oceanic arc (e.g., Kohistan arc in western Himalaya), the Gangdese arc is a prominent continental arc along the southern margin of Asia, and thus has more complex petrological architecture and geochemical composition due to ancient basement assimilation. The most noteworthy feature of this magmatic arc is its predominantly zircon $\varepsilon_{Hf}(t) > 0$ in the southern Lhasa terrane, and mostly zircon $\varepsilon_{Hf}(t) < 0$ in the central Lhasa terrane (e.g., Chu et al., 2006; Hou et al., 2015; Ji et al., 2009; Zhu et al., 2011). Although there have been many advances in the study of the Gangdese arc magmatism, important questions remain such as how this magmatic arc has been actually developed and what may have caused the across-arc zircon-Hf isotope systematics.

In this paper, we present bulk-rock major and trace element compositions, mineral chemistry, zircon geochronology, bulk-rock Sr—Nd and zircon Hf isotopic data on the igneous rocks, including Basong Tso cumulate plutons (<100 km^2) and Mamba MME-bearing granitoid batholith (>100 km^2) of ~200 Ma in the central Lhasa terrane in southern Tibet. Our results suggest that the amphibole-dominated assimilation–fractional crystallization (AFC) is the effective process for the generation of these Early Jurassic igneous rocks. This new understanding details a gradual crustal evolution with increasing mantle contribution of the central Lhasa terrane in the Mesozoic.

2. Geological background

The Tibetan Plateau, from north to south, comprises the Songpan-Ganzi flysch complex, Qiangtang and Lhasa terranes, and the Himalaya, separated by the Jinsha, Bangong-Nujiang and Indus-Yarlung Zangbo Suture zones, respectively (Fig. 1a; e.g., Dewey et al., 1988; Yin and Harrison, 2000; Zhu et al., 2013). As a main tectonic component, the

* Corresponding author at: Key Laboratory of Deep-Earth Dynamics of Ministry of Natural Resources, Institute of Geology, Chinese Academy of Geological Sciences, Beijing 100037, China.
E-mail address: dongxin5811935@163.com (X. Dong).

https://doi.org/10.1016/j.lithos.2020.105557

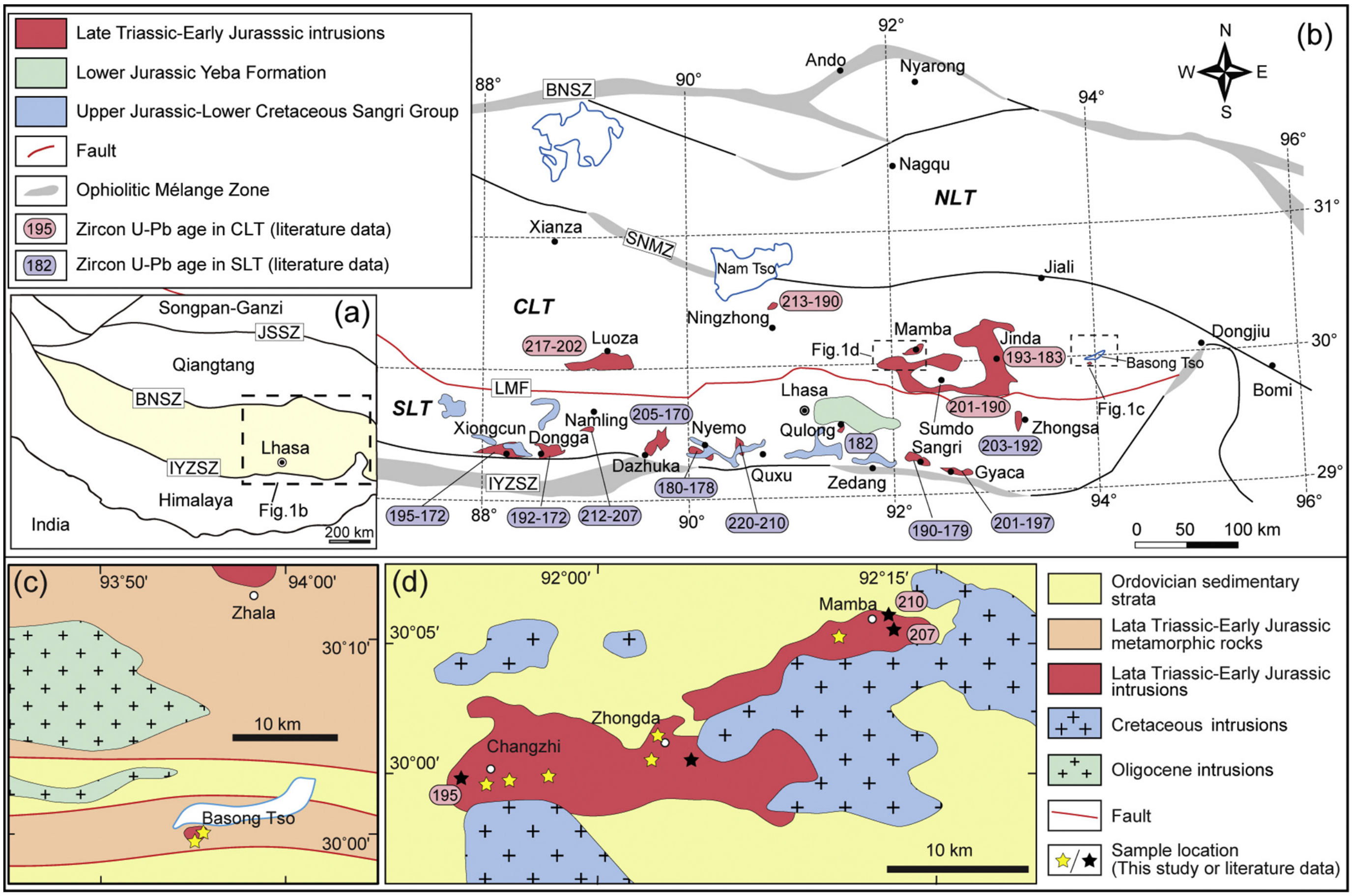

Fig. 1. (a) Tectonic framework of the Tibetan Plateau showing its major subdivisions (Zhu et al., 2013). (b) Schematic geological map of the central and eastern section of the Lhasa terrane modified from Pan et al. (2004), showing the study area, and the spatial and temporal distributions of the Late Triassic—Early Jurassic intrusive-volcano rocks in the central and southern Lhasa subterranes. (c) Geological map of the Basong Tso area. (d) Geological map of the Mamba area. Abbreviations: NLT = Northern Lhasa subterrane; CLT = Central Lhasa subterrane; SLT = Southern Lhasa subterrane; JSSZ = Jinsha Suture zone; BNSZ = Bangong-Nujiang Suture zone; IYZSZ = Indus-Yarlung Zangbo Suture zone; SNMZ = Shiquanhe-Nam Tso Mélange Zone; LMF = Luobadui-Mila Mountain Fault. Date sources: Zircon U—Pb ages in CLT (Luoza: 217–202 Ma, Chu et al., 2006; Zhang et al., 2007a; Ningzhong: 213–190 Ma, Kapp et al., 2005; Liu et al., 2006; Mamba: 210–195 Ma, He et al., 2006; Zhu et al., 2011; Sumdo: 201–190 Ma, Li et al., 2009a; Yu et al., 2018; Jinda: 193–183 Ma, Zhu et al., 2011), Zircon U—Pb ages in SLT (Xiongcun: 195–172 Ma, Lang et al., 2014a, 2014b; Qu et al., 2007; Tafti et al., 2009, 2014; Tang et al., 2010; Wang et al., 2017a; Xu et al., 2017a; Zou et al., 2015; Dongga: 192–172 Ma, Guo et al., 2013; Tan, 2012; Wang et al., 2017b; Xu et al., 2017b; Namling: 212–207 Ma, Ma et al., 2017; Dazhuka: 205–170 Ma, Chu et al., 2006; Guo et al., 2013; Ji et al., 2009; Meng et al., 2016b; Nyemo: 180–178 Ma, Guo et al., 2013; Meng et al., 2016b; Zhang et al., 2007b; Quxu: 220–210 Ma, Ma et al., 2018; Meng et al., 2016a; Qulong: 182 Ma, Yang et al., 2008; Sangri: 190–179 Ma, Dong and Zhang, 2013; Shui et al., 2018; Gyaca: 201–197 Ma, Dong and Zhang, 2013; Shui et al., 2018; Xu et al., 2019; Zhongsa: 203–192 Ma, Zhu et al., 2011).

Lhasa terrane in southern Tibet is interpreted to have been rifted from the northern margin of Gondwana in the Triassic and drifted northward to collide with the Qiangtang terrane in the Cretaceous (e.g., Zhu et al., 2013). An Andean-type active continental margin had been developed in the southern part of the terrane prior to its collision with the northward moving Indian continent in the Cenozoic (e.g., Dewey et al., 1988; Mo et al., 2008; Yin and Harrison, 2000; Zhu et al., 2011, 2013). The Lhasa terrane is subdivided into northern, central, and southern subterranes separated by the Shiquanhe-Nam Tso Mélange zone and the Luobadui-Mila Mountain fault, respectively (Fig. 1b; e.g., Pan et al., 2004; Zhu et al., 2011).

The southern Lhasa subterrane (SLT) is characterized by the existence of juvenile crust with a Precambrian metamorphic basement locally exposed (e.g., Dong et al., 2020; Ji et al., 2009; Mo et al., 2008; Zhu et al., 2011, 2013). This subterrane is dominated by the Cretaceous–Tertiary batholiths and the Paleogene Linzizong volcanic succession, with minor Triassic–Cretaceous volcano-intrusive rocks (Pan et al., 2004; Zhu et al., 2008, 2013). Several Early Paleozoic and Late Devonian granites have been reported in the eastern SLT (Dong et al., 2010, 2014; Ji et al., 2012; Ma et al., 2019). The central Lhasa subterrane (CLT) was once a microcontinent with Precambrian crystalline basement widely exposed (Dong et al., 2011a; Harris et al., 1988a; Li, 1955; Zhang et al., 2012), covered by Permo–Carboniferous metasedimentary rocks and Upper Jurassic–Lower Cretaceous strata with abundant volcanic-intrusive rocks, as well as minor Ordovician–Devonian, and Triassic strata (Pan et al., 2004; Zhu et al., 2009, 2011, 2013). The Mesozoic plutonic rocks occur as batholiths of varying age (cf. Zhu et al., 2011 and references therein). The volcanic rocks are mostly early Cretaceous in age with minor being Permian and Cambrian (e.g., Zhu et al., 2011, 2012). The Late Permian high-pressure Sumdo eclogite and Late Triassic–Early Jurassic metamorphic rocks in the middle and eastern CLT indicate subduction of the Sumdo Tethyan seafloor (e.g., Cheng et al., 2015; Dong et al., 2011b; Lin et al., 2013; Weller et al., 2015; Yang et al., 2009; Zeng et al., 2009). In the northern Lhasa subterrane (NLT), no basement rocks have been reported, and the oldest sedimentary cover is Middle Triassic sedimentary rocks (Pan et al., 2004; Zhu et al., 2011, 2013).

The Gangdese arc along the southern and central Lhasa subterranes, resulting from subduction of the Neo-Tethyan seafloor and subsequent India-Asia collision, extends E-W for >1500 km with varying width (~50 to 200 km; e.g., Zhu et al., 2015). Abundant age data indicate that these magmatic arc rocks were emplaced from the Late Triassic to the Late

Miocene (e.g., Zhu et al., 2011), with two main episodes of magmatic activity in the Late Triassic–Early Jurassic (220–170 Ma) and the Cretaceous (95–85 Ma) (e.g., Ji et al., 2009; Zhu et al., 2011). Except for those in the CLT, most plutonic rocks in the SLT have depleted zircon Hf and bulk-rock Sr—Nd isotopic compositions, indicative of significant mantle contributions or a juvenile crust in their petrogenesis (e.g., Mo et al., 2008; Zhu et al., 2011, 2013). The Early Mesozoic Gangdese arc formed in response to the northward subduction of the Neo-Tethyan seafloor to the south (e.g., Chu et al., 2006; Ji et al., 2009; Zhang et al., 2007b) or to the southward subduction of the Bangong–Nujiang Tethyan seafloor to the north (e.g., Shui et al., 2018; Zhu et al., 2011, 2013).

The samples of this study, part of Gangdese magmatic arc, were collected in the Basong Tso and Mamba areas of the CLT (Fig. 1c–d). In the Basong Tso area, the Early Jurassic and Oligocene plutons intrude the Ordovician strata and the Late Triassic—Early Jurassic metamorphic rocks (Figs. 1c and 2a). The latter metamorphic rocks experienced peak medium-pressure amphibolite-facies metamorphism related to the crustal thickening processes of the collision–accretion within the Lhasa terrane (Lin et al., 2013; Weller et al., 2015). The Early Jurassic Basong Tso plutons (about 6 km^2) include diorite and granodiorite cumulates, with the former intruding the latter (Fig. 2b–d). In the Mamba area, the Late Triassic—Early Jurassic batholith is about 130 km^2 in outcrop located northwest of the Sumdo eclogite (Fig. 1b), and intrudes the Ordovician strata (Figs. 1d and 3a) and has been intruded by the Late Cretaceous granitoids (Meng et al., 2014) (Fig. 1d). The Late Triassic—Early Jurassic Mamba batholith includes host granite, granodiorite and quartz monzodiorte (MME). MMEs widely occur as dark blobs of varying shape (ellipsoidal or elongate) and size (centimeters to decimeters) without chilled margins (Fig. 3b–d).

3. Petrography

This study focuses on the diorite and granodiorite cumulates from the Basong Tso area, and the MMEs and their host granites and granodiorite from the Mamba area. Sample details, including locations, lithology (based on mineral assemblages and modes), zircon U—Pb ages and $\varepsilon_{Hf}(t)$, bulk-rock $\varepsilon_{Nd}(t)$, are given in Table 1.

3.1. Basong Tso cumulates

The diorite cumulates display adcumulate texture, dominated by coarse-grained amphibole and plagioclase plus minor intercumulus material of titanite, apatite and biotite (Fig. 2e–f). Sample TD17–9-3 has similar mineral assemblage to other diorite cumulate samples with much less titanite. The granodiorite cumulates display porphyritic texture, including coarse-grained plagioclase and amphibole interlocked with quartz plus interstitial fine-grained quartz-feldspar, biotite, titanite and apatite (Fig. 2g). Within both types of cumulates, most minerals are partially altered with plagioclase replaced by sericite, amphibole by epidote and biotite by chlorite (Fig. 2e–g).

3.2. Mamba granitoids

The host rocks of the Mamba batholith include granite and granodiorite, showing medium-grained equigranular texture. The granites mainly consist of quartz, K-feldspar and plagioclase with minor biotite, amphibole and Fe-oxides (Fig. 3e). The granodiorite has similar mineral assemblage to the granite with less quartz and more amphibole (Fig. 3f–g). Quartz monzodiorte MMEs share the same mineralogy as the host granodiorite but have less quartz and finer grain size (Fig. 3h). The MMEs show heteradcumulate texture with higher modal amphibole poikilitically enclosed in plagioclase and K-feldspar plus minor interstitial quartz, biotite, titanite, apatite and Fe-oxides (Fig. 3i).

4. Analytical methods and data

Analytical methods are given in Supplementary Text 1, including cathodoluminescence (CL) images, mineral major elements, bulk-rock major and trace elements, Sr—Nd isotopes, zircon U—Pb dating and Hf isotopes.

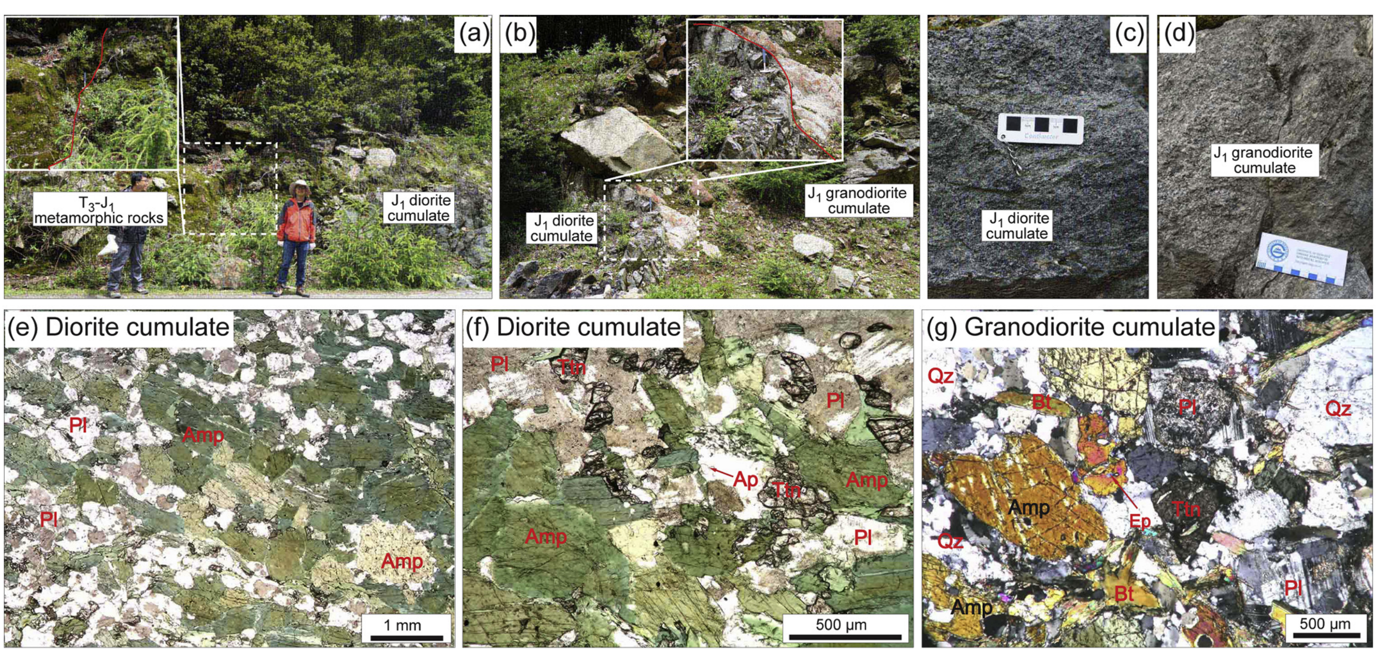

Fig. 2. Field photos and photomicrographs of representative diorite and granodiorite cumulates from the Basong Tso area. (a) The Early Jurassic (J_1) diorite cumulate intruding the Late Triassic—Early Jurassic (T_3-J_1) metamorphic rocks. (b) The Early Jurassic diorite cumulate intruding the granodiorite cumulate. (c) Outcrop of the Early Jurassic diorite cumulate. (d) Outcrop of the Early Jurassic granodiorite cumulate. (e) and (f) The mineral assemblage of diorite cumulate (under PPL). (g) The mineral assemblage of granodiorite cumulate (under XPL). Amp, amphibole; Ap, apatite; Bt, biotite; Ep, epidote; Pl, plagioclase; Qz, quartz; Ttn, titanite.

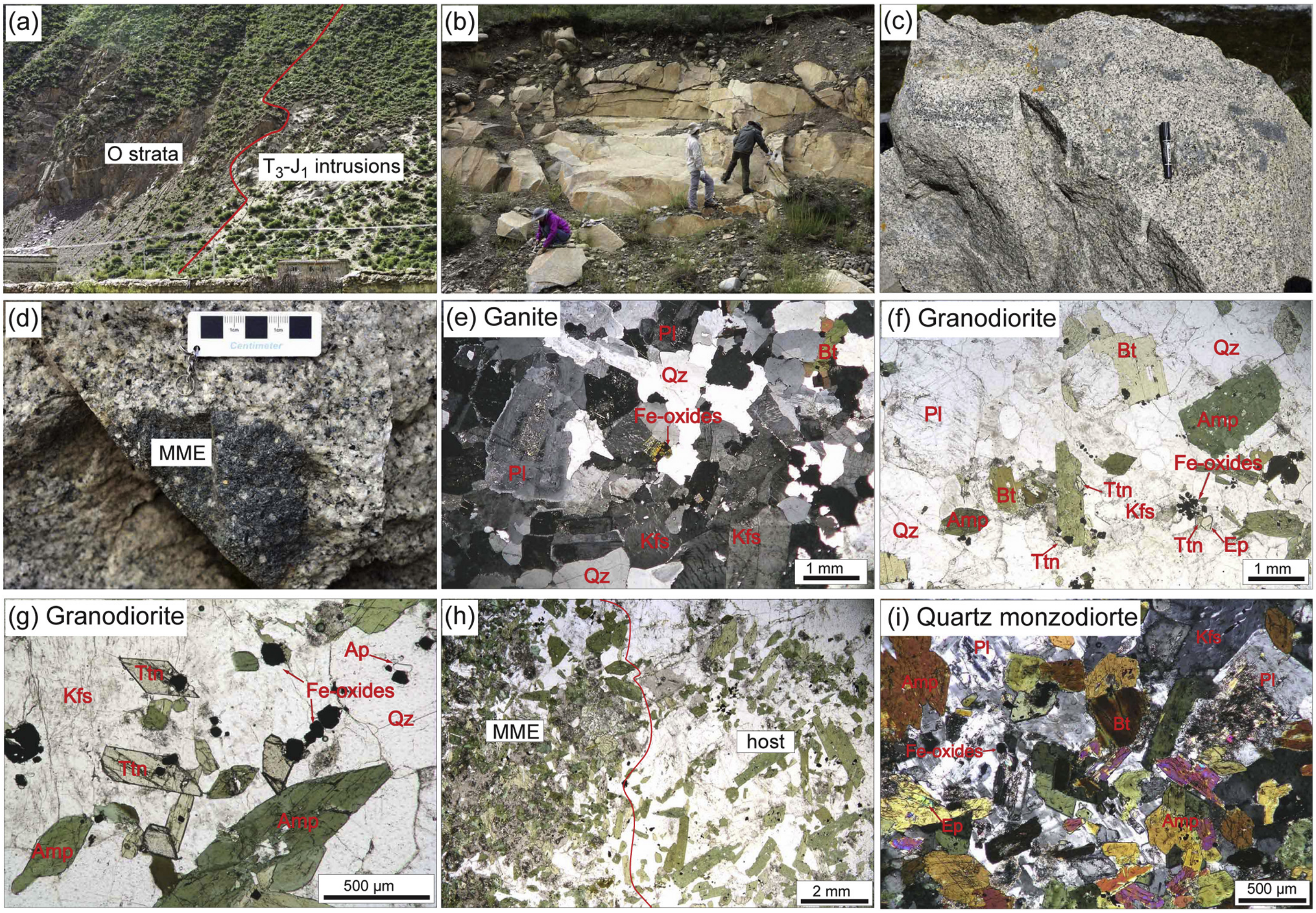

Fig. 3. Field photos and photomicrographs of granitoids from the Mamba area. (a) The Late Triassic—Early Jurassic granitoids intruding the Ordovician (O) strata. (b) Outcrop of the Mamba granitoids. (c) and (d) Outcrop showing the contact of MMEs of varying size within their host granitoids. (e) The mineral assemblage of the host granite (under XPL). (f) and (g) The mineral assemblage of the host granodiorite (under PPL). (h) The sharp contact between MME and their host rocks, showing MME being more fine-grained than the host rocks (under PPL). (i) The mineral assemblage of quartz monzodiorte MME (under XPL). Amp, amphibole; Ap, apatite; Bt, biotite; Ep, epidote; Kfs, K-feldspar; Pl, plagioclase; Qz, quartz; Ttn, titanite.

Table 1
Summary of sample characters and analytical results.

Sample	Lithology and mineral assemblage	Age (Ma)	Bulk-rock $\varepsilon_{Nd}(t)$	Zircon $\varepsilon_{Hf}(t)$	GPS Position
Basong Tso cumulate					
T12–25–1-1	Diorite cumulate, Amp (60–70%), Pl (25–35%), Ttn, Bt, Ap, Fe-oxides	190 ± 0.7	1.71	1.0 to 6.2	E93°54′42″; N30°0′12″
T12–25–1-2					E93°54′42″; N30°0′12″
TD17–9-2			1.57		E93°54′41″; N30°0′23″
TD17–9-3			−1.69		E93°54′41″; N30°0′23″
TD17–9-4			1.61		E93°54′41″; N30°0′23″
TD17–9-6			1.97		E93°54′41″; N30°0′23″
T12–25-4	Granodiorite cumulate, Pl (50%), Qz (20%), Amp (15%), Bt (5%), Ttn, Ap, Fe-oxides	198 ± 0.8		−14.1 to −3.8	E93°54′42″; N30°0′12″
T12–26-1		199 ± 1	−4.90	−12.8 to −6.3	E93°56′30″; N30°0′6″
X16–106-1					E93°54′42″; N30°0′12″
X16–106-2			−4.99		E93°54′42″; N30°0′12″
X16–106-3					E93°54′42″; N30°0′12″
TD17–9-8			−5.95		E93°54′41″; N30°0′23″
TD17–9-9			−5.06		E93°54′41″; N30°0′23″
Mamba granitoid					
T12–1-1	Host granite, Qz (35–40%), Kfs (20–25%), Pl (30–35%), Bt, ±Amp, Ap, Fe-oxides	190 ± 1			E91°55′36″; N29°59′53″
T12–2-1		189 ± 1		−2.8 to −0.8	E91°56′44″; N29°59′57″
T12–3-1		190 ± 1		−6.5 to 1.3	E91°58′2″; N30°0′10″
T12–4-1		189 ± 1		−5.2 to 1.7	E92°2′18″; N30°0′55″
T12–7-1		194 ± 1		−8.9 to −1.6	E92°10′36″; N30°5′20″
T12–9-1	Host granodiorite, Qz (25%), Kfs (20%), Pl (40%), Amp (10%), Bt, Ttn, Ap, Fe-oxides				E92°2′42″; N30°1′13″
T12–9-2	Quartz monzodiorte MME, Amp (30%), Kfs + Pl (60%), Qz, Bt, Ttn, Ap, Fe-oxides	190 ± 2		−3.0 to 3.7	E92°2′42″; N30°1′13″

Abbreviations: Amp, amphibole; Ap, apatite; Bt, biotite; Kfs, K-feldspar; Pl, plagioclase; Qz, quartz; Ttn, titanite.

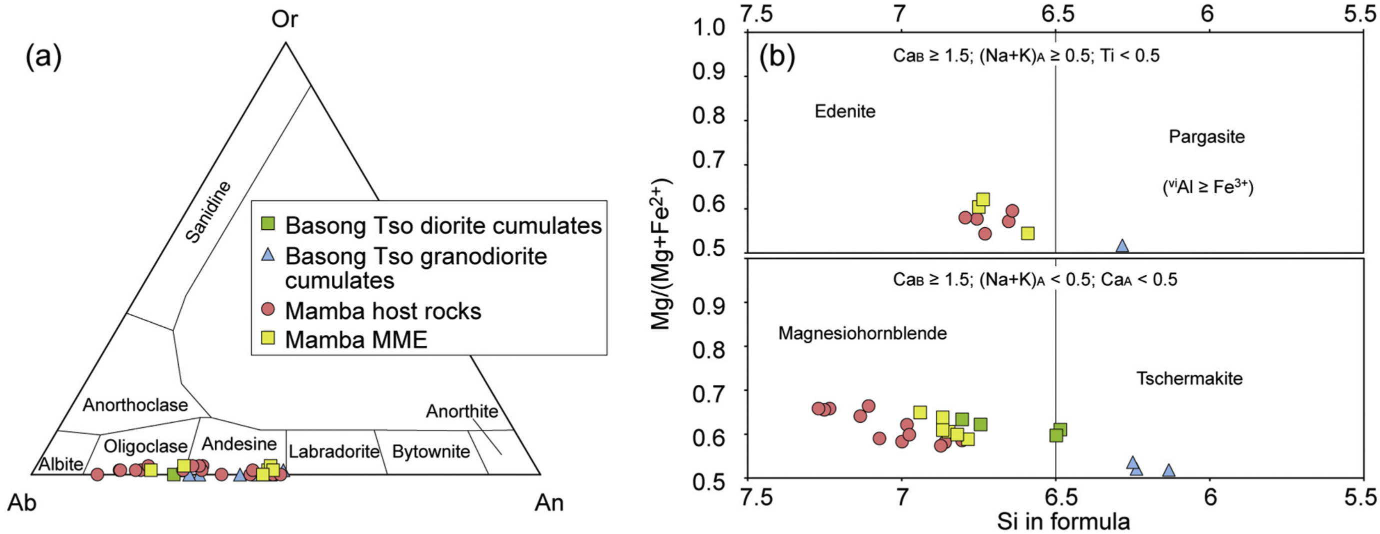

Fig. 4. Representative compositions of plagioclase and amphibole from the Early Jurassic intrusions in the central Lhasa subterrane. (a) Feldspar (anorthite (An)-albite (Ab)-orthoclase (Or)) compositional diagram from Deer et al. (1992). (b) Classification of amphiboles according to Leake et al. (1997).

4.1. Mineral compositions

Major element compositions for plagioclase and amphibole are given in Supplementary Table 1 and 2, respectively.

Plagioclase in the Basong Tso diorite and granodiorite cumulates has An = 28–49 (Fig. 4a). Plagioclase in the Mamba host rocks has varying composition with An = 13–46 (Fig. 4a), which is similar to that of the MMEs with An = 23–47 (Fig. 4a).

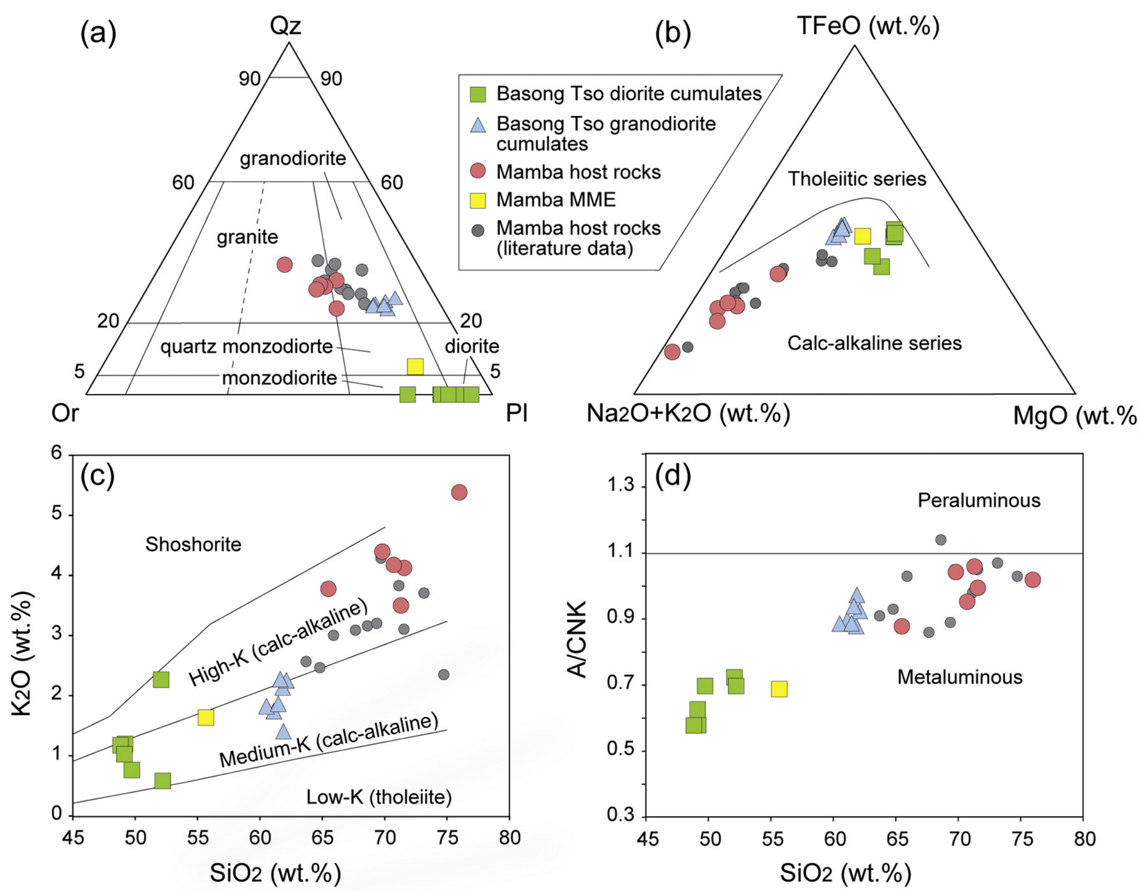

Fig. 5. Classification diagrams of the Early Jurassic intrusions in the central Lhasa subterrane. (a) Classification of the plutonic rocks using CIPW norms (Le Bas and Streckeisen, 1991). (b) AFM diagram after Wager and Deer (1939) with discriminatory lines of Irvine and Baragar (1971) dividing the calc-alkaline and tholeiitic magma series. (c) SiO_2 (wt%) vs K_2O (wt%) diagram (Peccerillo and Taylor, 1976). (d) SiO_2 (wt%) vs A/CNK diagram. Literature Data for the Late Triassic-Early Jurassic Mamba host rocks are from He et al. (2005, 2006).

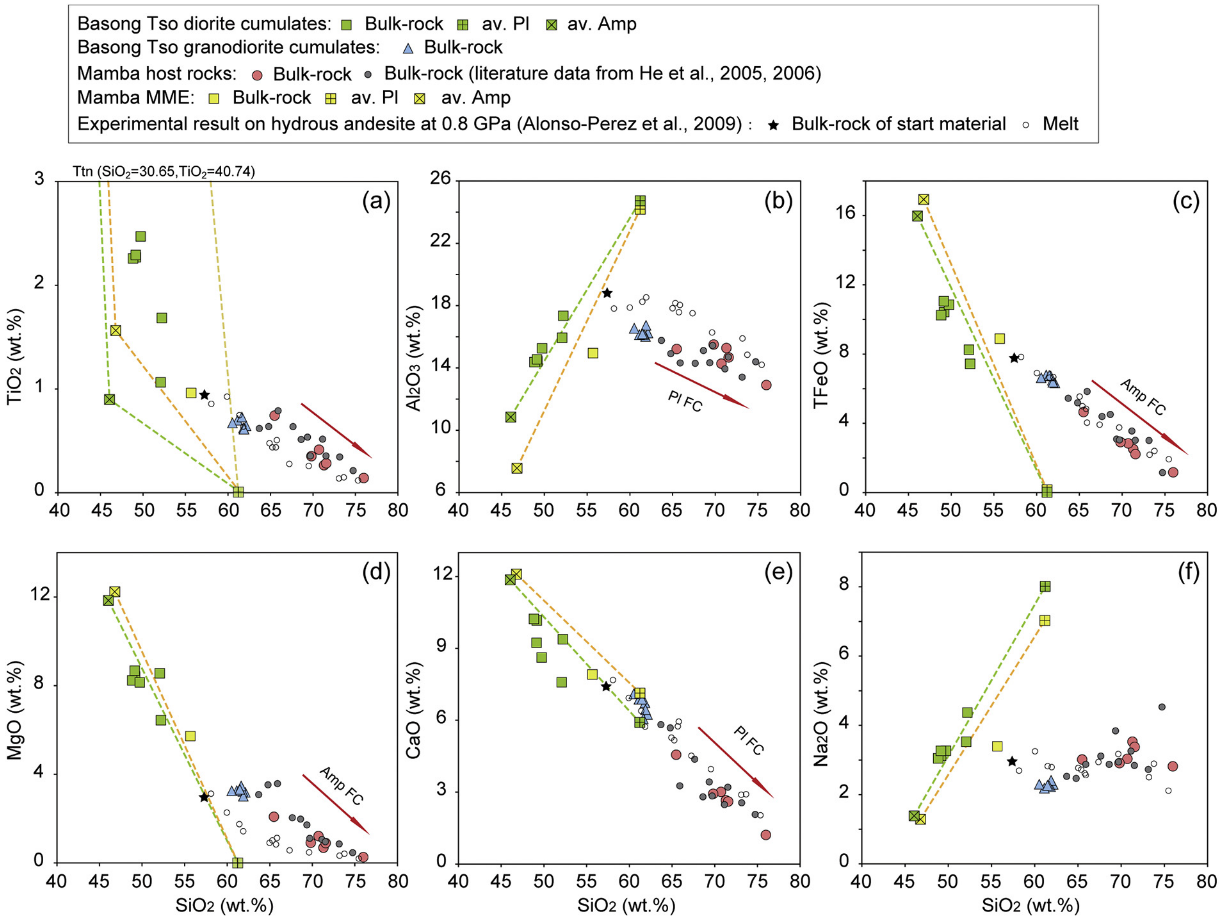

Fig. 6. SiO_2 variation diagrams of TiO_2, Al_2O_3, TFeO, MgO, CaO and Na_2O (wt%) for the Early Jurassic intrusions in the central Lhasa subterrane. Bulk-rock: bulk-rock major element compositions; av. Pl: average plagioclase major element compositions; av. Amp: average amphibole major element compositions; Bulk-rock of start material: bulk-rock major element compositions of experimental starting material; Melt: experimentally determined major element compositions of equilibrium crystallization melt.

Amphibole is the dominant mafic mineral in all samples except for Mamba host sample T12–1-1. All amphibole is calcic with $Ca_{Bsite} = 1.742–1.971$ (Leake et al., 1997), but shows additional compositional variation, seeing Fig. 4b.

4.2. Bulk-rock major and trace element and Sr—Nd isotope data

Bulk-rock major element, trace element and Sr—Nd isotopic compositions of the studied samples are given in Supplementary Table 3.

4.2.1. Basong Tso cumulates

The diorite cumulates with low SiO_2 (47.6–51.2 wt%) show linear trends (except for TiO_2) on SiO_2-variation diagrams (Figs. 5 and 6). The granodiorite cumulates have higher SiO_2 (59.8–60.7 wt%) and limited range for other oxides (Fig. 6). The diorite cumulates are enriched in light rare earth elements (LREEs) relative to heavy REEs (HREEs) with fractionated REE patterns and weak negative Eu anomalies (Fig. 7a). Most samples display positive Nb and Ta anomalies without negative Ti anomaly (except for sample TD17–9-3 with negative Nb, Ta and Ti anomalies in Fig. 7b, probably due to less titanite modes seeing 3.1 above). The granodiorite cumulates have similar REE patterns (Fig. 7c), but show negative U, Nb, Ta and Ti anomalies (Fig. 7d). Both types of cumulates have varying Nb/Ta of 12.43–24.12.

For diorite and granodiorite cumulates, their initial $^{87}Sr/^{86}Sr$ isotopic ratios and $\varepsilon_{Nd}(t)$ values are calculated at 190 and 200 Ma, respectively (using the zircon age data, see 4.3 below). The diorite cumulates have $(^{87}Sr/^{86}Sr)_i$ of 0.7059–0.7088 and $\varepsilon_{Nd}(t)$ of −1.69 to +1.97 (Fig. 8). The granodiorite cumulates have $(^{87}Sr/^{86}Sr)_i$ of 0.7061–0.7067 and lower $\varepsilon_{Nd}(t)$ of −5.95 to −4.90 (Fig. 8).

4.2.2. Mamba granitoids

The Mamba host rocks have varying SiO_2 (64.4–75.3 wt%), equivalent to granodiorite and granite (Fig. 5a), belonging to high-K calc-alkaline series with metaluminous characteristics (Fig. 5b–d). Their other major elements show variations inversely correlated with SiO_2 (Fig. 6a–e) (except for Na_2O, Fig. 6f). The MME has low SiO_2 (54.5 wt%) with major element composition similar to that of the Basong Tso cumulates (Figs. 5b–d and 6).

The host rocks have enriched LREEs relative to HREEs with fractionated REE patterns (the most depleted HREEs are Ho and its neighbors with $[Dy/Lu]n = 0.6–1.1$) and weak negative Eu anomalies (Fig. 7e), and show significant negative Ba, Nb, Sr, P and Ti anomalies (Fig. 7f). The MME has relatively higher middle and heavy REEs than the host rocks, similar to the Basong Tso granodiorite cumulates (Fig. 7e–f).

4.3. Zircon U—Pb age and Hf isotope

LA-ICP-MS zircon U—Pb dating on nine samples and Hf isotope compositions of eight samples are given in Supplementary Tables 4 and 5, respectively.

4.3.1. Basong Tso cumulates

Zircons from one diorite cumulate sample are euhedral short-prismatic with varying size (~50–100 μm), exhibiting weak magmatic

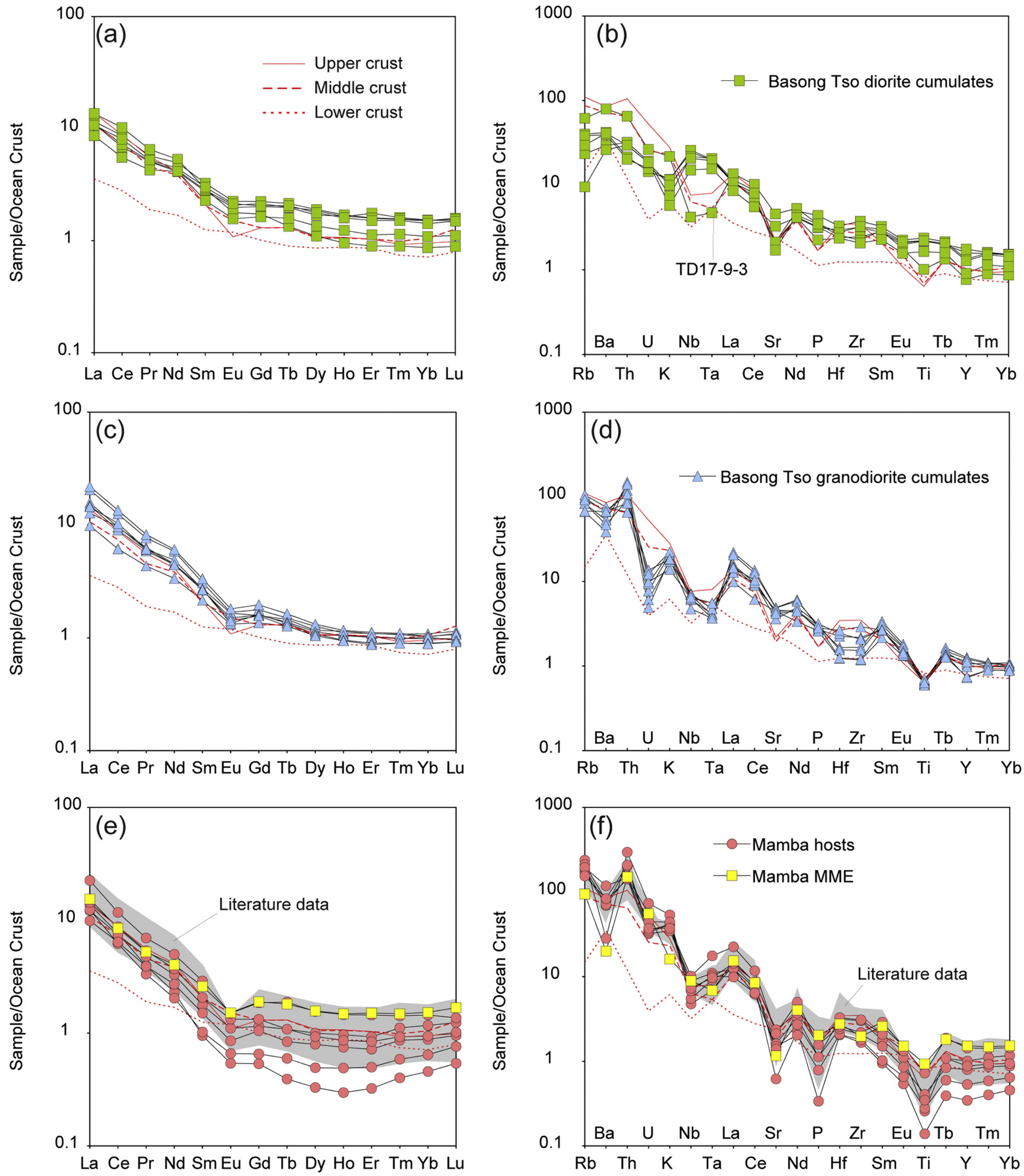

Fig. 7. Ocean crust-normalized REE and ocean crust-normalized multi-element patterns for the Early Jurassic intrusions in the central Lhasa subterrane. (a) and (b) Diorite cumulate from the Basong Tso area. (c) and (d) Granodiorite cumulate from the Basong Tso area. (e) and (f) Host granitoids and MME from the Mamba area. Literature data for the Late Triassic-Early Jurassic Mamba host rocks are from He et al. (2005, 2006); Average ocean crust composition are from Niu and O'Hara (2003); Data of upper, middle and lower crust are from Rudnick and Gao (2003).

oscillatory zonation (Fig. 9a). Analyzed spots give weighted mean $^{206}Pb/^{238}U$ age of 190 ± 0.7 Ma (Fig. 10a). Thirteen Hf isotopic analyses give $\varepsilon_{Hf}(t) > 0$, ranging from +1.0 to +6.2 (Fig. 11).

Zircons from two granodiorite cumulate samples are euhedral prismatic with varying size (~200–300 μm) and oscillatory zoning of magmatic origin (Fig. 9b and c). Analyzed spots give weighted mean $^{206}Pb/^{238}U$ ages of 198 ± 0.8 and 199 ± 1 Ma (Fig. 10b and c). Their 34 Hf isotopic analyses give $\varepsilon_{Hf}(t) < 0$, ranging from −14.1 to −3.8 (Fig. 11).

4.3.2. Mamba granitoids

Zircons from five host granite samples are similar to those of the Basong Tso granodiorite cumulates (Fig. 9d–h). Analyzed spots give weighted mean $^{206}Pb/^{238}U$ ages of 194–189 Ma (Fig. 10d–h). Their 62 Hf isotopic analyses give varying $\varepsilon_{Hf}(t)$ from −8.9 to +1.7 (Fig. 11).

Zircons from the MME sample are also of magmatic origin with varying size (~50–200 μm) (Fig. 9i). Analyzed spots give weighted mean $^{206}Pb/^{238}U$ age of 190 ± 2 Ma (Fig. 10i). Their 38 Hf isotopic analyses give varying $\varepsilon_{Hf}(t)$ from −3.0 to +3.7 (Fig. 11).

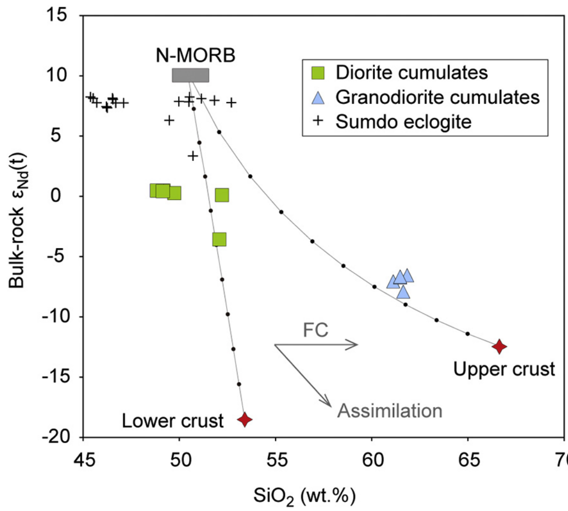

Fig. 8. Bulk-rock SiO_2 (wt%) vs $\varepsilon_{Nd}(t)$ for the Early Jurassic diorite and granodiorite cumulates from the Basong Tso area in the central Lhasa subterrane. The data of the Sumdo eclogite are from Li et al. (2009b) and Zeng et al. (2009). Binary mixing calculations are between N-MORB (average composition of $\varepsilon_{Nd}(t) = 10.04$, $SiO_2 =$ 50.46 wt%, Nd = 11.32 ppm are from Niu et al. (2002b)) and lower crust (average composition of $\varepsilon_{Nd}(t) = -18.52$ is from Othman et al. (1984), $SiO_2 = 53.4$ wt% and Nd = 11 ppm are from Rudnick and Gao (2003)), and upper crust (average composition of $\varepsilon_{Nd}(t) = -12.40$ is from Harris et al. (1988b), $SiO_2 = 66.6$ wt% and Nd = 27 ppm are from Rudnick and Gao (2003)). The mixing lines are calculated after Faure (1977) with 10% intervals shown.

5. Discussion

5.1. Petrogenesis of the Early Jurassic igneous rocks in the central Lhasa subterrane

The age data on magmatic zircons from our samples indicate that the Basong Tso diorite and granodiorite cumulates crystallized at ca. 190 and 199–198 Ma, respectively; the Mamba MMEs formed coevally with their host rocks at ca. 190 and 194–189 Ma. We discuss the petrogenesis of these Early Jurassic igneous rocks respectively below.

5.1.1. Basong Tso cumulates

The Basong Tso diorite cumulates with typical adcumulate texture (e.g., Wager et al., 1960) are most consistent with an origin by crystal accumulation of amphibole, plagioclase and titanite from mafic andesitic magmas. Bulk-rock compositions of cumulate rocks are controlled by both compositions and modes of the constituent minerals (Niu et al., 2002a). Indeed, most major element oxides define trends between average compositions of plagioclase and amphibole, except for TiO_2 as the result of heterogeneous distribution of titanite (Fig. 6). Fig. 6a shows that the bulk-rock composition lies in space defined by titanite-plagioclase-amphibole assemblage. Moreover, the high Nb and Ta (Supplementary Table 3) and their significant positive anomalies in Fig. 7 are consistent with high amphibole modes (e.g., Tiepolo et al., 2000). Importantly, the major mineralogy of amphibole + plagioclase indicates that their parental

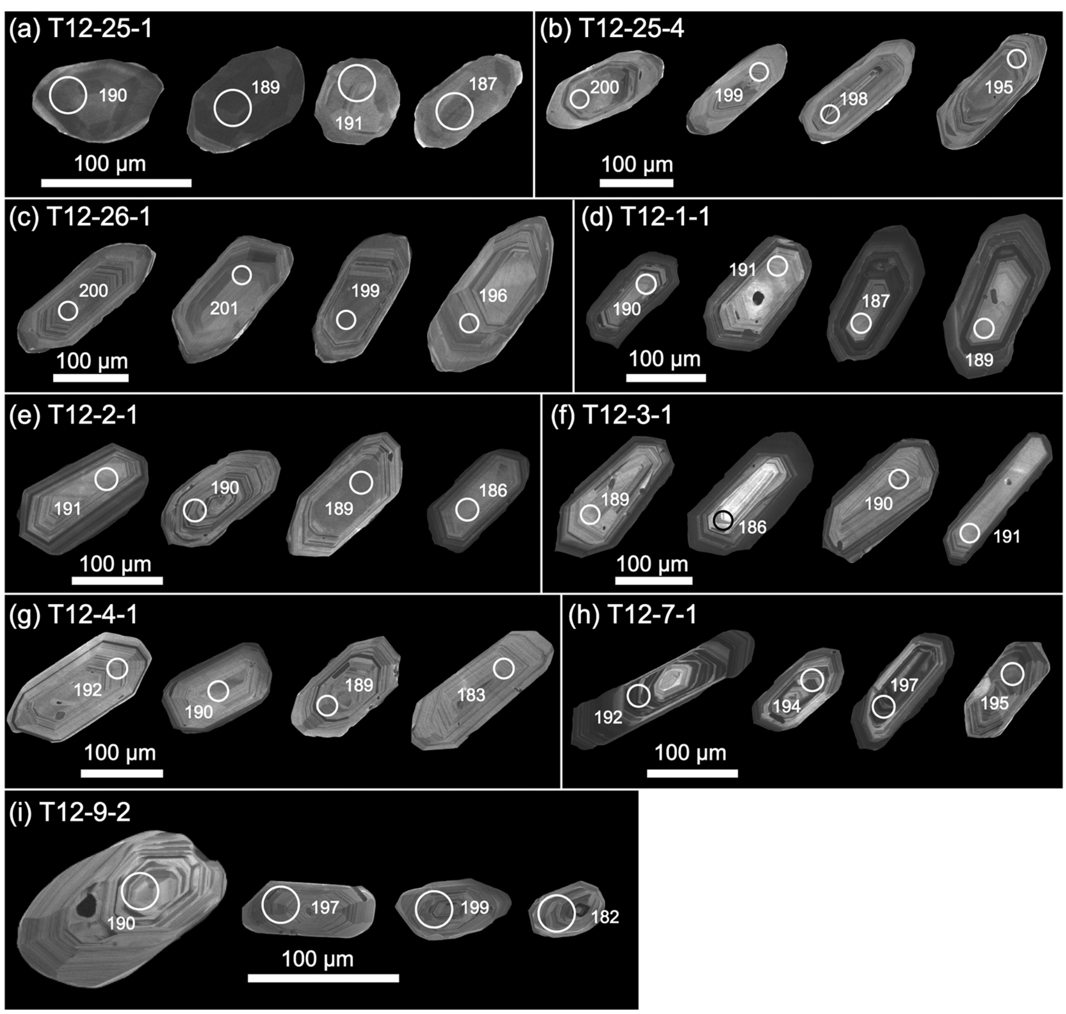

Fig. 9. Cathodoluminescence images of the representative zircons of the Early Jurassic intrusions in the central Lhasa subterrane. The circles are the analytical spots with ages in Ma.

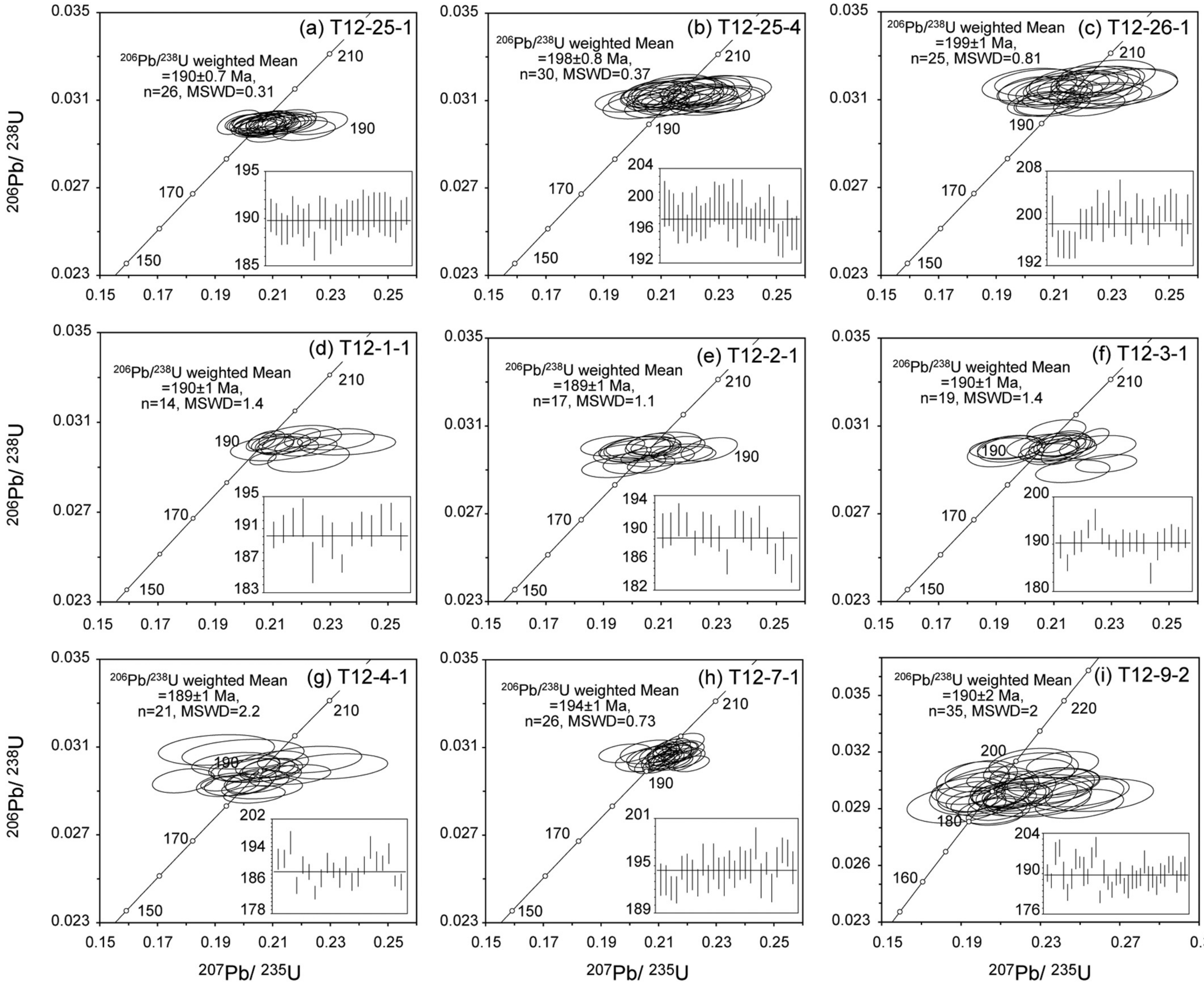

Fig. 10. Zircon U—Pb concordia diagrams for the Early Jurassic intrusions in the central Lhasa subterrane.

melts must be mafic andesitic magmas (e.g., Alonso-Perez et al., 2009; Niu et al., 2013).

The granodiorite cumulates show porphyritic texture that has been reported in cumulate rocks (e.g., Schaen et al., 2018; Xu et al., 2019). These rocks comprise a framework of touching euhedral-subhedral minerals dominated by amphibole along with plagioclase (Fig. 2g), suggesting the earlier-formed cumulus (e.g., Irvine, 1982). The fine-grained interstitial assemblage represents trapped melt (e.g., Schaen et al., 2018). Moreover, the high Nb/Ta (up to 24.12, Supplementary Table 3) is also consistent with amphibole control because of $Kd_{Amp}^{Nb/Ta}=1.40$ (e.g., Foley et al., 2002). Due to high viscosity, the crystal-melt separation is likely incomplete. Thus, the Basong Tso granodiorite cumulates are likely crystal-rich mixtures with trapped SiO_2-rich melt, which explains why the granodiorite cumulates have higher SiO_2 than diorite cumulates.

5.1.2. Mamba granitoids

5.1.2.1. Mamba host rocks. With increasing viscosity in high-SiO_2 melt, crystal separation becomes more ineffective. We suggest that the Mamba host rocks are melt-rich mixtures with incompletely segregated crystals, which explain their major element compositional systematics as a function of SiO_2 (Fig. 6a–e). These geochemical characteristics are consistent with melt compositions of equilibrium crystallization experiment results of hydrous andesite related to amphibole fractionation (Fig. 6, Alonso-Perez et al., 2009). The amphibole fractional crystallization leads to reduction of TFeO, MgO and Dy/Yb with increasing SiO_2 in the residual melt (Figs. 6c, d and 12a), and also results in spoon-shaped REE patterns with varying lower Tb, Dy, Ho and Er (Fig. 7e) (amphibole preferentially incorporates middle REEs over heavy REEs; Davidson et al., 2007). Meanwhile, fractional crystallization of plagioclase can effectively deplete Al_2O_3, CaO, Eu (Figs. 6b, e and 12b) and Ba and Sr in the evolving magma (Fig. 7f). Therefore, the Mamba host rock compositional systematics is consistent with andesitic magmas that have undergone amphibole-plagioclase fractional crystallization.

5.1.2.2. Mamba MME. Controversy exists on the MME petrogenesis, including foreign xenoliths (e.g., Vernon, 1983), partial melting residues of the source rocks (e.g., Chappell et al., 1987), magma mixing between mantle-derived basaltic magma and crust-derived felsic magma (e.g., Didier, 1987), and earlier cumulate crystallized from the same magmatic system (e.g., Donaire et al., 2005). In this study, the Mamba MME sample has typical magmatic textures in both field and petrographic observations without peraluminous minerals (Fig. 3d, h, i) and

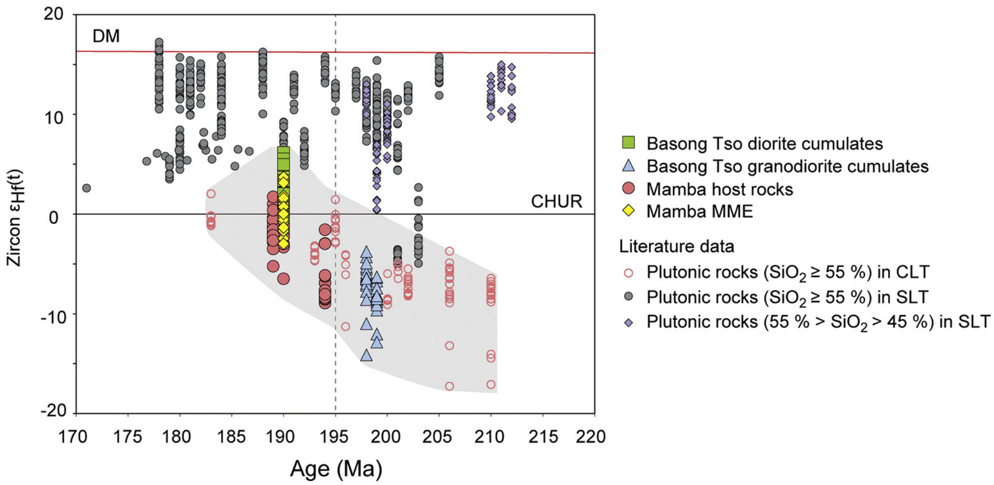

Fig. 11. Zircon U—Pb ages vs ε_{Hf}(t) diagram for the Late Triassic–Early Jurassic intrusions from the central and southern Lhasa subterranes. Abbreviations: DM = depleted mantle; CHUR = chondritic uniform reservoir. Data sources: Plutonic rocks ($SiO_2 \geq 55\%$) in the CLT are from Zhang et al. (2007a), Zhu et al. (2011) and Yu et al. (2018); Plutonic rocks ($SiO_2 \geq 55\%$) in the SLT are from Chu et al. (2006), Dong and Zhang (2013), Guo et al. (2013), Ji et al. (2009), Meng et al. (2016b), Shui et al. (2016, 2018), Xu et al. (2019), Yang et al. (2011), Zhang et al. (2007b) and Zhu et al. (2011); Plutonic rocks ($55\% > SiO_2 > 45\%$) in the SLT are from Meng et al. (2016a), Shui et al. (2018) and Xu et al. (2019).

formed coevally with their host rocks (Table 1), ruling out the foreign xenolith and restite origins. For MMEs formed by magma mixing, there are some common characteristics, (1) distinguishable isotopic contrast between the MMEs and the host rocks; (2) disequilibrium textures of the MMEs, e.g., complex zoning of clinopyroxene (e.g., Wang et al., 2013) or reversed zoning of plagioclase (e.g., Shcherbakov et al., 2011). However, none of the above typical evidence for magma mixing is observed. Instead, the MMEs have cumulate textures, and their bulk-rock compositions are mainly controlled by those of amphibole-plagioclase (Fig. 6). Moreover, the MMEs and their host rocks have the same mineral assemblage, similar mineral (plagioclase and amphibole) compositions and overlapping zircon ε_{Hf}(t) values (Figs. 3h, 4 and 11). Therefore, the MMEs represent earlier cumulate derived from cogenetic magma with their host rocks.

5.2. Constraints on the source

The Early Jurassic cumulates (Basong Tso cumulates and Mamba MME) in the CLT comprise dominantly amphibole and plagioclase that are common cumulate crystals of andesitic melts, whereas the typical cumulate from evolved basaltic melt would be gabbro dominated by clinopyroxene and plagioclase (Niu et al., 2013). Moreover, the compositions of the Mamba host granitoids are consistent with melt compositions of equilibrium crystallization experiment results of hydrous andesite (Fig. 6, Alonso-Perez et al., 2009). Thus, the primary magmas parental to the studied Early Jurassic igneous rocks are mafic andesite. In addition, our bulk-rock ε_{Nd}(t) (−5.95 to +1.97) and zircon ε_{Hf}(t) (−14.1 to +6.2) isotopic data indicate significant mantle or juvenile mafic crust contribution to the granitoid magmatism. Moreover, the positive correlation of La/Sm with SiO_2 (Fig. 12c) further indicates crustal assimilation to be important, which is understood to be inevitable in terms of crustal melting or magma chamber processes. Generally, the source for the andesitic parental magmas with mantle isotopic signature could be (1) evolved mantle-derived basaltic magmas; (2) juvenile mafic continental crust derived from the mantle in no distant past; and possibly (3) the underplated ocean crust. Firstly, it is inadequate to produce huge granitoid batholiths, such as the Mamba batholith, through basaltic magma evolution. Moreover, fractional crystallization of basaltic magmas generates mafic or ultramafic cumulate (e.g., gabbro mentioned above; or garnet pyroxenite, Lee et al., 2006), both of which are absent in the studied areas. Secondly, no related juvenile mafic continental rocks have been reported so far, except for ca. 492 Ma basalts with negative

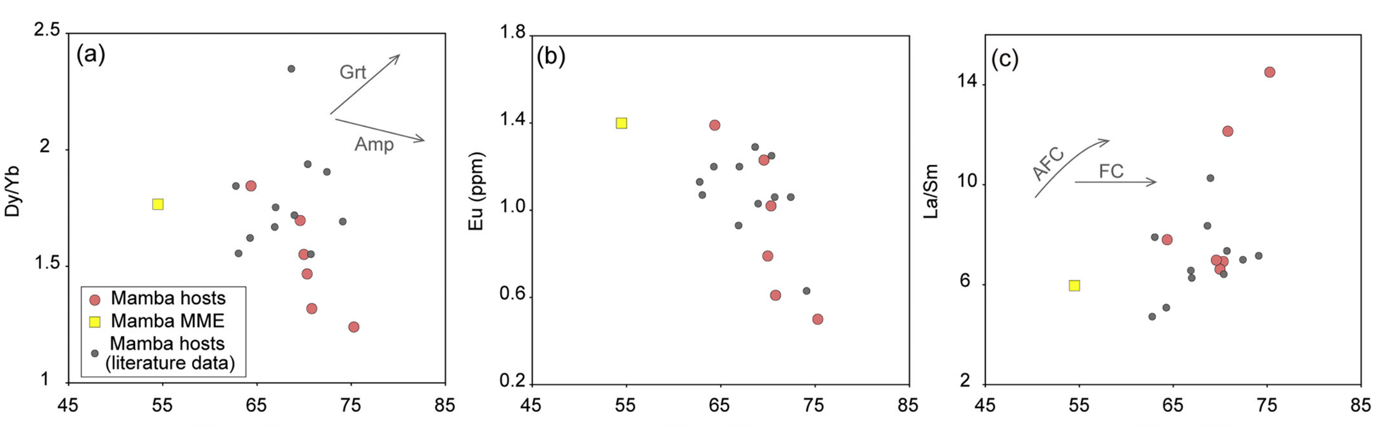

Fig. 12. SiO_2 (wt%) variation diagrams of Dy/Yb, Eu (ppm) and La/Sm for the Early Jurassic intrusions from the Mamba area in the central Lhasa subterrane. Literature data for the Late Triassic—Early Jurassic Mamba host rocks are from He et al. (2005, 2006).

bulk-rock $\varepsilon_{Nd}(t)$ in the CLT (Zhu et al., 2012). Therefore, we suggest that the most likely origin for the andesitic magma parental to the studied Early Jurassic igneous rocks is partial melting of the remaining Late Paleozoic Sumdo Tethyan ocean crust represented by the Sumdo eclogite that had exhumated to the middle-lower crust at ca. 200 Ma (e.g., Cheng et al., 2015). The remaining ocean crust could undergo partial melting to produce andesitic melt under amphibolite-facies conditions (cf. Niu et al., 2013 and references therein). Moreover, the coeval metamorphic conditions (9 kbar at ca. 204–192 Ma, Weller et al., 2015) of the country rocks indicated that the magmas parental to the Basong Tso cumulates were formed at the middle-lower crustal depths. This possibility has also been suggested by Zhu et al. (2011).

The model of partial melting of the remaining ocean crust and the recycled terrigenous sediments has been proposed and tested by Niu and co-workers in many orogenic belts (e.g., Chen et al., 2016; Huang et al., 2014; Mo et al., 2008; Niu et al., 2013). We suppose that the geodynamic trigger for the Early Mesozoic magmatism of the Lhasa terrane is the northward subduction of the Neo-Tethyan seafloor beneath the Lhasa terrane (e.g., Chu et al., 2006; Ji et al., 2009; Zhang et al., 2007b). During seafloor subduction, mantle wedge flow supplies heat and maintains to heat the underplated hydrated ocean crust and related continental material that would melt together to generate the andesitic magmas parental to the studied Early Jurassic igneous rocks with inherited mantle isotopic signatures.

5.3. Late Triassic–early Jurassic magmatism of the Lhasa terrane

The Late Triassic–Early Jurassic magmatic rocks are widely scattered in the entire SLT and central–eastern CLT (Fig. 1b). In the SLT, the Early Mesozoic magmatic rocks include plutonic and volcanic rocks. The plutonic rocks mainly include diorite, tonalite, granodiorite and granite with minor hornblende gabbro, and their bulk-rock geochemical data are characterized by medium-K calc-alkaline and metaluminous, typical of I-type granitoids with zircon $\varepsilon_{Hf}(t) > 0$ (e.g., Guo et al., 2013; Meng et al., 2016a, 2016b; Shui et al., 2018; Xu et al., 2019; Zhu et al., 2011). In the CLT, the Early Mesozoic magmatic rocks occur as batholiths in the eastern CLT and plutons in the central CLT (Fig. 1b). The batholiths near Mamba, Sumdo and Jinda areas are I-type granodiorite and granite with MMEs, compositionally medium- to high-K calc-alkaline and metaluminous, with variable zircon $\varepsilon_{Hf}(t)$ values (He et al., 2005, 2006; Yu et al., 2018; Zhu et al., 2011; this study). By comparison, the plutons near Luoza and Ningzhong areas mainly consist of peraluminous S-type granite with zircon $\varepsilon_{Hf}(t) < 0$ (Chu et al., 2006; Liu et al., 2006; Zhang et al., 2007b).

5.4. Crustal evolution of the Lhasa terrane

The crust in the Lhasa terrane has been considered to be dominated by ancient crust in the CLT, but dominated by younger juvenile crust in the SLT and NLT as manifested by zircon Hf and bulk-rock Nd isotope compositions of the granitoids (e.g., Hou et al., 2015; Zhu et al., 2011). Zircon Hf isotope has been used as a useful tool for understanding continental crust formation and evolution (e.g., Kinny and Maas, 2003). Here we show zircon $\varepsilon_{Hf}(t)$ values from the Early Mesozoic plutonic rocks (~215–170 Ma) in the SLT and CLT. Fig. 11 shows that granitoids from the SLT have zircon $\varepsilon_{Hf}(t) > 0$, whereas granitoids in the CLT have zircon $\varepsilon_{Hf}(t)$ varying systematically from $\varepsilon_{Hf}(t) < 0$ at ca. 210 Ma towards $\varepsilon_{Hf}(t) > 0$ at ca. 195 Ma. Spatially, from north to south, zircon

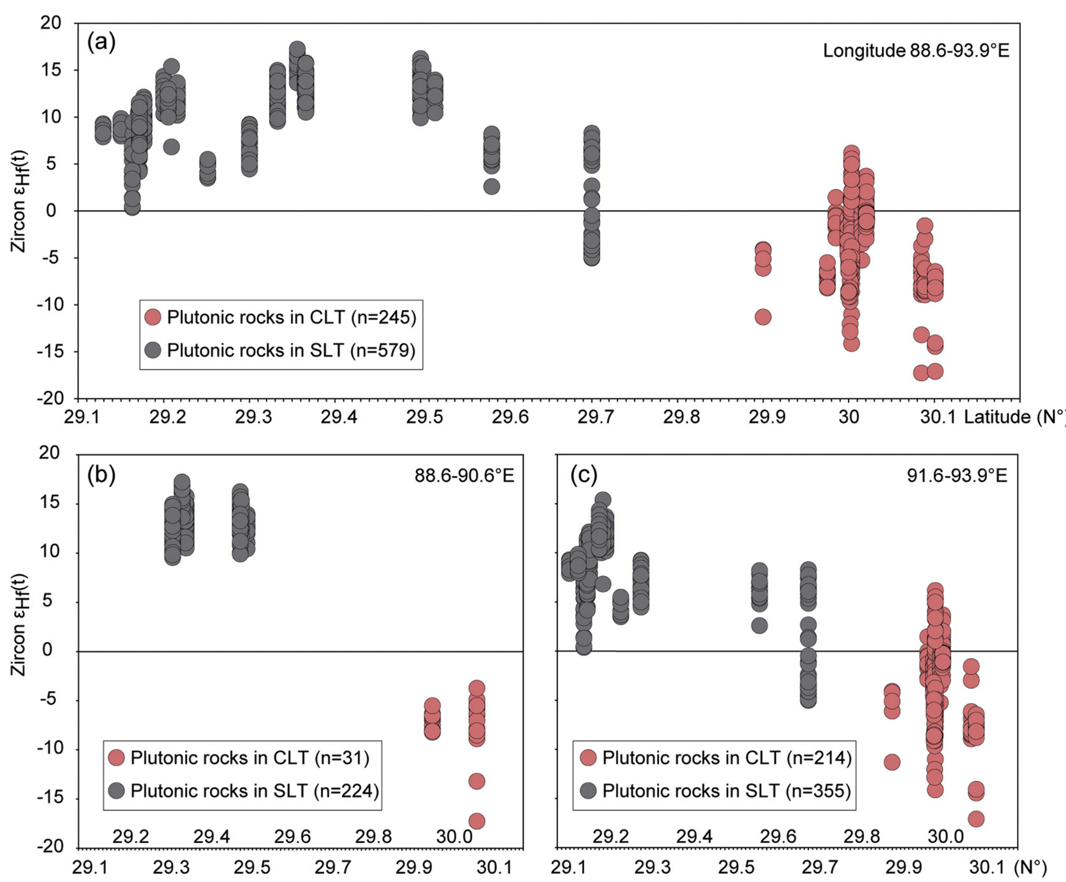

Fig. 13. The range and spatial distribution of zircon $\varepsilon_{Hf}(t)$ from the Late Triassic—Early Jurassic (~215–170 Ma) intrusions in the central and southern Lhasa subterranes. (a) Zircon $\varepsilon_{Hf}(t)$ plotted against sample latitude of 29.1° — 30.2°N at the longitude of 88.6–93.9°E. (b) Zircon $\varepsilon_{Hf}(t)$ plotted against sample latitude of 29.1° — 30.2°N at longitude of 88.6–90.6°E. (c) Zircon $\varepsilon_{Hf}(t)$ plotted against sample latitude of 29.1° — 30.2°N at longitude of 91.6–93.9°E. Data sources are the same as in Fig. 11.

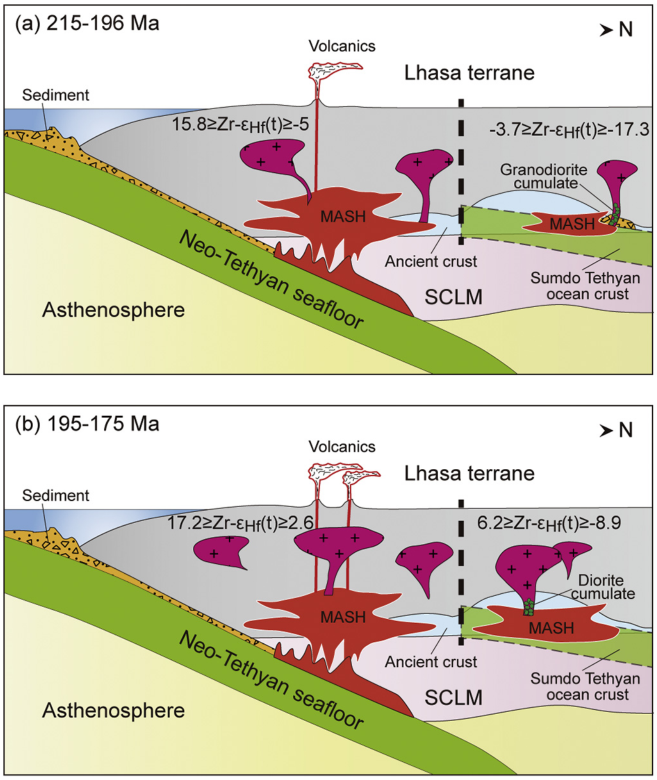

Fig. 14. Cartoons showing the Late Triassic—Early Jurassic magmatism and crustal evolution in the central and southern Lhasa subterranes. (a) During 215–196 Ma, magmas in the SLT are derived from mantle with minor ancient crustal assimilation at the northernmost; magmas in the CLT are derived from hydrated ocean crust together with much subducted sediments. (b) During 195–175 Ma, magmas in the SLT are derived from mantle with much less ancient crustal assimilation; magmas in the CLT are derived from much more hydrated ocean crust together with ancient crust. Zircon ε_{Hf}(t) data sources are the same as in Fig. 11. Black dashed line shows the subterrane bounding between the SLT and the CLT, i.e., Luobadui-Mila Mountain Fault zone in Fig. 1b. Abbreviations: SCLM = subcontinental lithospheric mantle; MASH = melting-assimilation-storage-homogenization zone.

ε_{Hf}(t) values gradually increase, i.e., from $\varepsilon_{Hf}(t) < 0$ in the CLT to $\varepsilon_{Hf}(t) > 0$ southward in Fig. 13. It is well understood that crust–mantle interaction is inevitable during source melting (e.g., melting of subducted sediments) and magma emplacement (e.g., crustal assimilation).

Here, we suggest that although mantle material contribution (juvenile or remelting of mantle-derived rocks) is important, significant melt assimilation with ancient crustal material results in the signature of $\varepsilon_{Hf}(t) < 0$ in the northernmost CLT in the Late Triassic, then melting of abundant recycled terrigenous sediments of upper continental crust and remaining of the Sumdo Tethyan ocean crust in the melting region generates the andesitic magma parental to the ca. 200 Ma granodiorite cumulates (Fig. 14a). With the CLT magmatism getting younger and southward, melting of much more Sumdo Tethyan ocean crust with adjacent ancient lower crust forms the parental magmas of the ca. 190 Ma diorite cumulates and MME-bearing granitoid, when the zircon ε_{Hf}(t) gradually increases towards positive values, reflecting increasing mantle contribution (Fig. 14b). Notedly, zircon ε_{Hf}(t) of the granitoids from the CLT are all negative at longitude 88.6–90.6° E (Fig. 13b), which is consistent with S-type granitoids of crustal re-working origin (see above 5.3). For the coeval plutonic rocks of the SLT, zircon Hf isotope also shows signatures of the crustal assimilation, representing the wide range of zircon ε_{Hf}(t) at ca. 205–200 Ma (Fig. 11) and values around zero at latitude ca. 29.7° N (Fig. 13a and c). Our study supports Zhu et al. (2011) that granitoids from the SLT are dominated by mantle contributions up to 50–90%, but those from the CLT has much less mantle contribution (0–60%) (Fig. 8). Ma et al. (2019) recently showed that the SLT already experienced growth with juvenile crust in the Paleozoic and was once a microcontinent with Precambrian basement but transformed into juvenile terrane over time. We suggest that the crustal evolution is a multi-episode and gradual process. For the CLT, the multiple plutonic rocks record the Early Mesozoic crustal evolution with increasing mantle contribution with time as manifested by increasing zircon ε_{Hf}(t) values.

6. Conclusion

(1) The Early Jurassic igneous rocks in the CLT include the Basong Tso plutons of diorite cumulate (ca. 190 Ma), granodiorite cumulate (ca. 200 Ma) and the Mamba batholith of host granitoids and MMEs with the same crystallization age (~190 Ma).
(2) The Basong Tso plutons are formed by crystal accumulation of amphibole, plagioclase and titanite from a mafic andesitic magma. The Mamba host granitoids are formed through amphibole-plagioclase fractional crystallization of an andesitic magma. The MMEs share the same mineralogy and indistinguishable isotopic compositions with their host granitoids, indicating earlier cumulate from the same magmatic system as their host rocks.
(3) The parental magma for the Early Jurassic igneous rocks with inherited mantle isotopic signatures is best understood as resulting from partial melting of the hydrated ocean crust together with varying continental material.
(4) The multiple plutonic rocks (~215–170 Ma) in the CLT record the Early Mesozoic crustal evolution of the Lhasa terrane, characterized by increasing mantle contribution reflected by gradual increase of zircon ε_{Hf}(t) with time. The SLT had already experienced juvenile crustal growth in the Paleozoic.

Declaration of Competing Interest

The authors declare that they have no known competing financial interests or personal relationships that could have appeared to influence the work reported in this paper.

Acknowledgement

We want to thank two anonymous journal referees and Editor-in-Chief Xian-Hua Li for their constructive comments, which clearly helped to improve the quality of this paper. This study was co-supported by the National Key Research and Development Project of China (2016YFC0600310), the National Natural Science Foundation of China (grant 41872070 and 91855210) and Basic Science and Technology Research Fundings of the Institute of Geology, CAGS (grant J2006). Xin Dong acknowledges the China Scholarship Council for funding a 12-month research at Durham University, UK (CSC NO. 201809110024). We thank Dr. Yanhao Lin, Zhijia Chen, Huixia Ding and Yanfei Chen, PhD. student Shengkai Qin for taking part in field work.

Appendix A. Supplementary data

Supplementary data to this article can be found online at https://doi.org/10.1016/j.lithos.2020.105557.

References

Alonso-Perez, R., Müntener, O., Ulmer, P., 2009. Igneous garnet and amphibole fractionation in the roots of island arcs: experimental constraints on andesitic liquids. Contrib. Mineral. Petrol. 157, 541–558.
Chappell, B., White, A., Wyborn, D., 1987. The importance of residual source material (restite) in granite petrogenesis. J. Petrol. 28, 1111–1138.
Chen, S., Niu, Y.L., Li, J.Y., Sun, W.L., Zhang, Y., Hu, Y., Shao, F.L., 2016. Syn-collisional adakitic granodiorites formed by fractional crystallization: insights from their

enclosed mafic magmatic enclaves (MMEs) in the Qumushan pluton, North Qilian Orogen at the northern margin of the Tibetan Plateau. Lithos 248–251, 455–468.
Cheng, H., Liu, Y., Vervoort, J.D., Lu, H., 2015. Combined U-Pb, Lu-Hf, Sm-Nd and Ar-Ar multichronometric dating on the Bailang eclogite constrains the closure timing of the Paleo-Tethys Ocean in the Lhasa terrane, Tibet. Gondw. Res. 28, 1482–1499.
Chu, M.F., Chung, S.L., Song, B., Liu, D.Y., O'Reilly, S.Y., Pearson, N.J., Ji, J.Q., Wen, D.J., 2006. Zircon U-Pb and Hf isotope constraints on the Mesozoic tectonics and crustal evolution of southern Tibet. Geology 34, 745–748.
Davidson, J., Turner, S., Handley, H., Dosseto, A., 2007. Amphibole "sponge" in arc crust? Geology 35, 787–790.
Deer, W.A., Howie, R.A., Zussman, J., 1992. An Introduction to the Rock-Forming Minerals. 2nd edition. Longman Group, Harlow, pp. 1–232.
Dewey, J.F., Shackleton, R.M., Chang, C., Sun, Y., 1988. The tectonic evolution of the Tibetan Plateau. Philos. Trans. R. Soc. Lond. A 327, 379–413.
Didier, J., 1987. Contribution of enclave studies to the understanding of origin and evolution of granitic magmas. Geol. Rundsc. 76, 41–50.
Donaire, T., Pascual, E., Pin, C., Duthou, J.L., 2005. Microgranular enclaves as evidence of rapid cooling in granitoid rocks: the case of the Los Pedroches granodiorite, Iberian Massif, Spain. Contrib. Mineral. Petrol. 149, 247–265.
Dong, X., Zhang, Z.M., 2013. Genesis and tectonic significance of the Early Jurassic magmatic rocks from the southern Lhasa terrane. Acta Petrol. Sin. 29, 1933–1948 (in Chinese with English abstract).
Dong, X., Zhang, Z.M., Santosh, M., 2010. Zircon U–Pb chronology of the Nyingtri Group, Southern Lhasa Terrane, Tibetan Plateau: implications for Grenvillian and Pan-African provenance and Mesozoic-Cenozoic metamorphism. J. Geol. 118, 677–690.
Dong, X., Zhang, Z.M., Santosh, M., Wang, W., Yu, F., Liu, F., 2011a. Late Neoproterozoic thermal events in the northern Lhasa terrane, South Tibet: Zircon chronology and tectonic implications. J. Geodyn. 52, 389–405.
Dong, X., Zhang, Z.M., Liu, F., He, Z.Y., Lin, Y.H., 2014. Late Paleozoic intrusive rocks from the southeastern Lhasa terrane, Tibetan Plateau, and their Late Mesozoic metamorphism and tectonic implications. Lithos 198–199, 249–262.
Dong, X., Zhang, Z.M., Liu, F., Wang, W., Yu, F., Shen, K., 2011b. Zircon U–Pb geochronology of the Nyainqêntanglha Group from the Lhasa terrane: new constraints on the Triassic orogeny of the south Tibet. J. Asian Earth Sci. 42, 732–739.
Dong, X., Zhang, Z.M., Niu, Y.L., Tian, Z.L., Zhang, L.L., 2020. Reworked Precambrian metamorphic basement of the Lhasa terrane, southern Tibet: Zircon/Titanite U–Pb geochronology, Hf isotope and Geochemistry. Precambrian Res. 336, 105496.
Faure, G., 1977. Principles of Isotope Geology. John Wiley and Sons, USA.
Foley, S., Tiepolo, M., Vannucci, R., 2002. Growth of early continental crust controlled by melting of amphibolite in subduction zones. Nature 417, 837–840.
Guo, L.S., Liu, Y.L., Liu, S.W., Cawood, P.A., Wang, Z.H., Liu, H.F., 2013. Petrogenesis of Early to Middle Jurassic granitoid rocks from the Gangdese belt, Southern Tibet: implications for early history of the Neo-Tethys. Lithos 179, 320–333.
Harris, N.B.W., Holland, T.J.B., Tindle, A.G., 1988a. Metamorphic rocks of the 1985 Tibet Geotraverse, Lhasa to Golmud. Philos. Trans. R. Soc. Lond. A 327, 203–213.
Harris, N.B.W., Xu, R.H., Lewis, C.L., Hawkesworth, C.L., Zhang, Y.Q., 1988b. Isotope geochemistry of the 1985 Tibet Geotraverse, Lhasa to Golmud. Philos. Trans. R. Soc. Lond. A 327, 263–285.
He, Z.H., Yang, D.M., Zheng, C.Q., Huang, Y.C., 2005. Geochemistry of the Indosinian granitoids in the Mamba area, Gangdise belt, Tibet and its tectonic significance. Geol. Bull. China 24, 354–359 (in Chinese with English abstract).
He, Z.H., Yang, D.M., Zheng, C.Q., Wang, T.W., 2006. Isotopic dating of the Mamba granitoid in the Gangdise tectonic belt and its constraint on the subduction time of the Neotethys. Geol. Rev. 52, 100–106 (in Chinese with English abstract).
Hou, Z.Q., Duan, L., Lu, Y.J., Zheng, Y.C., Zhu, D.C., Yang, Z.M., Yang, Z.S., Wang, B.D., Pei, Y.R., Zhao, Z.D., McCuaig, T.C., 2015. Lithospheric architecture of the Lhasa terrane and its control on ore deposits in the Himalayan–Tibetan orogen. Econ. Geol. 110, 1541–1575.
Huang, H., Niu, Y.L., Nowell, G., Zhao, Z.D., Yu, X.H., Zhu, D.C., Mo, X.X., Ding, S., 2014. Geochemical constraints on the petrogenesis of granitoids in the East Kunlun Orogenic belt, northern Tibetan Plateau: implications for continental crust growth through syn-collisional felsic magmatism. Chem. Geol. 370, 1–18.
Irvine, T.N., 1982. Terminology for layered intrusions. J. Petrol. 23, 127–162.
Irvine, T.N., Baragar, W.R.A., 1971. A guide to the chemical classification of the common volcanic rocks. Can. J. Earth Sci. 8, 523–548.
Jagoutz, O., Kelemen, P.B., 2015. Role of Arc Processes in the Formation of Continental Crust. Annu. Rev. Earth Planet. Sci. 43, 363–404.
Ji, W.Q., Wu, F.Y., Chung, S.L., Li, J.X., Liu, C.Z., 2009. Zircon U-Pb geochronology and Hf isotopic constraints on petrogenesis of the Gangdese batholith, southern Tibet. Chem. Geol. 262, 229–245.
Ji, W.Q., Wu, F.Y., Liu, C.Z., Chung, S.L., 2012. Identification of early Carboniferous granitoids from southern Tibet and implications for terrane assembly related to the Paleo-Tethyan evolution. J. Geol. 120, 531–541.
Kapp, J.L.D., Harrison, T.M., Kapp, P., Grove, M., Lovera, O.M., Lin, D., 2005. Nyainqentanglha Shan: a window into the tectonic, thermal, and geochemical evolution of the Lhasa block, southern Tibet. J. Geophys. Res. Solid Earth 110 (B08413), 2005. https://doi.org/10.1029/2004JB003330.
Kinny, P.D., Maas, R., 2003. Lu-Hf and Sm-Nd isotope systems in zircon zircon. In: Hanchar, J.M., Hoskin, P.W.O. (Eds.), Reviews in Mineralogy and Geochemistry. 53, pp. 327–341.
Lang, X.H., Tang, J.X., Li, Z.J., Huang, Y., Ding, F., Yang, H.H., Xie, F.W., Zhang, L., Wang, Q., Zhou, Y., 2014a. U-Pb and Re-Os geochronological evidence for the Jurassic porphyry metallogenic event of the Xiongcun district in the Gangdese porphyry copper belt, southern Tibet, PRC. J. Asian Earth Sci. 79, 608–622.
Lang, X.H., Tang, J.X., Xie, F.W., Li, Z.J., Huang, Y., Ding, F., Yang, H.H., Zhou, Y., Wang, Q., 2014b. Geochronology and geochemistry of the southern porphyry in the Xiongcun district and its geological implications, Tibet. Geotect. Metall. 38, 609–620 (in Chinese with English abstract).
Le Bas, M.J., Streckeisen, A.L., 1991. The IUGS systematics of igneous rocks. J. Geol. Soc. London 148, 825–833.
Leake, B.E., Woolley, A.R., Arps, C.E.S., other 19 co-authors, 1997. Nomenclature of amphiboles: report of the subcommittee on amphiboles of the International Mineralogical Association. Commission on New Minerals and Mineral Names. Can. Mineral. 35, 219–246.
Lee, A.Cin-Ty, Cheng, X., Horodyskyj, U., 2006. The development and refinement of continental arcs by primary basaltic magmatism, garnet pyroxenite accumulation, basaltic recharge and delamination: insights from the Sierra Nevada, California. Contrib. Mineral. Petrol. 151, 222–242.
Li, P., 1955. Primary understanding of geology, eastern Tibet. Chin. Sci. Bull. 7, 62–71 (in Chinese).
Li, H.Q., Xu, Z.Q., Yang, J.S., Cai, Z.H., Chen, S.Y., Tang, Z.M., 2009a. Records of Indosinian orogenesis in Lhasa Terrane, Tibet. J. Earth Sci. 20, 348–363.
Li, Z.L., Yang, J.S., Xu, Z.Q., Li, T.F., Xu, X.Z., Ren, Y.F., Robinson, O.T., 2009b. Geochemistry and Sm-Nd and Rb-Sr isotopic composition of eclogite in the Lhasa terrane, Tibet, and its geological significance. Lithos 109, 240–247.
Lin, Y.H., Zhang, Z.M., Dong, X., Xiang, H., Yan, R., 2013. Early Mesozoic metamorphism and tectonic significance of the eastern segment of the Lhasa terrane, south Tibet. J. Asian Earth Sci. 78, 160–183.
Liu, Q.S., Jiang, W., Jian, P., Ye, P.S., Wu, Z.H., Hu, D.G., 2006. Zircon SHRIMP U-Pb age and petrochemical and geochemical features of Mesozoic muscovite monzonitic granite at Ningzhong, Tibet. Acta Petrol. Sin. 22, 643–652 (in Chinese with English Abstract).
Ma, S.W., Meng, Y.K., Xu, Z.Q., Liu, X.J., 2017. The discovery of late Triassic mylonitic granite and geologic significance in the middle Gangdese batholiths, southern Tibet. J. Geodyn. 104, 49–64.
Ma, X.X., Meert, J.G., Xu, Z.Q., Yi, Z.Y., 2018. Late Triassic intra-oceanic arc system within Neotethys: evidence from cumulate appinite in the Gangdese belt, southern Tibet. Lithosphere 10, 545–565.
Ma, L., Kerr, A.C., Wang, Q., Jiang, Z.Q., Tang, G.J., Yang, J.H., Xia, X.P., Hu, W.L., Yang, Z.Y., Sun, P., 2019. Nature and evolution of crust in southern Lhasa, Tibet: Transformation from microcontinent to juvenile terrane. J. Geophys. Res. Solid Earth 124, 6452–6474.
Meng, F.Y., Zhao, Z., Zhu, D.C., Mo, X.X., Guan, Q., Huang, Y., Dong, G.C., Zhou, S., DePaolo, D.J., Harrison, T.M., Zhang, Z.C., Liu, J.L., Liu, Y.S., Hu, Z.C., Yuan, H.L., 2014. Late Cretaceous magmatism in Mamba area, central Lhasa subterrane: products of back-arc extension of Neo-Tethyan Ocean? Gondw. Res. 26, 505–520.
Meng, Y.K., Xu, Z.Q., Santosh, M., Ma, X.X., Chen, X.J., Guo, G.L., Liu, F., 2016a. Late Triassic crustal growth in southern Tibet: evidence from the Gangdese magmatic belt. Gondw. Res. 37, 449–464.
Meng, Y.K., Dong, H.W., Cong, Y., Xu, Z.Q., Cao, H., 2016b. The early-stage evolution of the Neo-Tethys Ocean: evidence from granitoids in the middle Gangdese batholith, southern Tibet. J. Geodyn. 94–95, 34–49.
Mo, X.X., Niu, Y.L., Dong, G.C., Zhao, Z.D., Hou, Z.Q., Zhou, S., Ke, S., 2008. Contribution of syncollisional felsic magmatism to continental crust growth: a case study of the Paleogene Linzizong volcanic Succession in southern Tibet. Chem. Geol. 250, 49–67.
Niu, Y.L., Gilmore, T., Mackie, S., Greig, A., Bach, W., 2002a. Mineral chemistry, whole-rock compositions, and petrogenesis of Leg 176 gabbros: data and discussion. In: Natland, J.H., et al. (Eds.), Proceedings of the Ocean Drilling Program Scientific Results. 176, pp. 1–69.
Niu, Y.L., O'Hara, M.J., 2003. Origin of ocean island basalts: a new perspective from petrology, geochemistry, and mineral physics considerations. J. Geophys. Res. 108 (2209), 2003. https://doi.org/10.1029/2002JB002048.
Niu, Y.L., Regelous, M., Wendt, J.I., Batiza, R., O'Hara, M.J., 2002b. Geochemistry of near-EPR seamounts: importance of source vs. process and the origin of enriched mantle component. Earth Planet. Sci. Lett. 199, 327–345.
Niu, Y.L., Zhao, Z.D., Zhu, D.C., Mo, X.X., 2013. Continental collision zones are primary sites for net continental crust growth—a testable hypothesis. Earth-Sci. Rev. 127, 96–110.
Othman, D.B., Polvé, M., Allègre, C.J., 1984. Nd-Sr isotopic composition of granulites and constraint on the evolution of the lower continental crust. Nature 307, 510–515.
Pan, G.T., Ding, J., Yao, D., Wang, L., 2004. Geological Map of the Qinghai–Xizang (Tibet) Plateau and Adjacent Areas. Chengdu Cartographic Publishing House, Chengdu (in Chinese).
Peccerillo, R., Taylor, S.R., 1976. Geochemistry of eocene calc-alkaline volcanic rocks from the Kastamonu area, Northern Turkey. Contrib. Mineral. Petrol. 58, 63–81.
Qu, X.M., Xin, H.B., Xu, W.Y., 2007. Collation of age of ore-hosting volcanics in Xiongcun superlarge Cu-Au deposit on basis of three zircon U-Pb SHRIMP ages. Miner. Depos. 26, 512–518 (in Chinese with English abstract).
Rudnick, R.L., 1995. Making continental crust. Nature 378, 571.
Rudnick, R.L., Gao, S., 2003. Composition of the continental crust. In: Rudnick, R.L. (Ed.), Treatise on Geochemistry. The Crust 3. Elsevier, pp. 1–64.
Schaen, A.J., Singer, B.S., Cottle, J.M., Garibali, N., Schoene, B., Satkoski, A.M., Fournelle, J., 2018. Textural and mineralogical record of low-pressure melt extraction and silicic cumulate formation in the late Miocene Risco Bayo–Huemul plutonic complex, southern Andes. J. Petrol. 59, 1991–2016.
Shcherbakov, V.D., Plechov, P.Y., Izbekov, P.E., Shipman, J.S., 2011. Plagioclase zoning as an indicator of magma processes at bezymianny volcano, Kamchatka. Contrib. Mineral. Petrol. 162, 83–99.
Shui, X.F., He, Z.Y., Zhang, Z.M., Lu, T.Y., 2016. Magma origin of Early Jurassic tonalites in the Eastern Gangdese Magmatic Belt, southern Tibet and its implications for the crustal evolution of the Lhasa Terrane. Acta Geol. Sin. 90, 3129–3152 (in Chinese with English abstract).
Shui, X.F., He, Z.Y., Klemd, R., Zhang, Z.M., Lu, T.Y., Yan, L.L., 2018. Early Jurassic adakitic rocks in the southern Lhasa sub-terrane, southern Tibet: petrogenesis and geodynamic implications. Geol. Mag. 155, 132–148.

Tafti, R., Mortensen, J.K., Lang, J.R., Rebagliati, M., Oliver, J.L., 2009. Jurassic U-Pb and Re-Os ages for the newly discovered Xietongmen Cu-Au porphyry district, Tibet, PRC: implications for metallogenic epochs in the southern Gangdese belt. Econ. Geol. 104, 127–136.

Tafti, R., Lang, J.R., Mortensen, J.K., Oliver, J.L., Rebagliati, C.M., 2014. Geology and geochronology of the Xietongmen (Xiongcun) Cu-Au porphyry district, Southern Tibet, China. Econ. Geol. 109, 1967–2001.

Tan, C.C., 2012. The Age and Petrogenesis of the Dongga Intrusion in the Gangdese Magmatic Belt, North Xigaze. (Master Thesis). China University of Geosciences, Beijing, pp. 1–73 (in Chinese with English abstract).

Tang, J.X., Li, F.J., Li, Z.J., Zhang, L., Tang, X.Q., Deng, Q., Lang, X.H., Huang, Y., Yao, X.F., Wang, Y., 2010. Period of time for the formation of main geologic bodies in Xiongcun copper-gold deposit, Xietongmen County, Tibet: evidence from Zircon U-Pb ages and Re-Os ages of molybdenite. Miner. Depos. 29, 461–475 (in Chinese with English abstract).

Taylor, S.R., McLennan, S.M., 1985. The Continental Crust: Its Composition and Evolution. Blackwell, Oxford, p. 312.

Tiepolo, M., Vannucci, R., Oberti, R., Foley, S., Bottazzi, P., Zanetti, A., 2000. Nb and Ta incorporation and fractionation in titanian pargasite and kaersutite: crystal-chemical constraints and implications for natural systems. Earth Planet. Sci. Lett. 176, 185–201.

Vernon, R.H., 1983. Restite, xenoliths and microgranitoid enclaves in granites. J. Proc. R. Soc. New South Wales 116, 77–103.

Wager, L.R., Deer, W.A., 1939. Geological investigation in East Greenland, Part III, the petrology of the Skaergaard intrusion, Kangerdluqssuaq, East Greenland. Meddelser Gronland 105.

Wager, L.R., Brown, G.M., Wansworth, W.J., 1960. Types of igneous cumulates. J. Petrol. 1, 73–85.

Wang, Q., Li, X.H., Jia, X.H., Wyman, D., Tang, G.J., Li, Z.X., Ma, L., Yang, Y.H., Jiang, Z.Q., Gou, G.N., 2013. Late Early cretaceous adakitic granitoids and associated magnesian and potassium-rich mafic enclaves and dikes in the Tunchang–Fengmu area, Hainan Province (South China): partial melting of lower crust and mantle, and magma hybridization. Chem. Geol. 328, 222–243.

Wang, R., Tafti, R., Hou, Z.Q., Shen, Z.C., Guo, N., Evans, N.J., Jeon, H., Li, Q.Y., Li, W.K., 2017a. Across-arc geochemical variation in the Jurassic magmatic zone, Southern Tibet: implication for continental arc-related porphyry Cu-Au mineralization. Chem. Geol. 451, 116–134.

Wang, R.Q., Qiu, J.S., Yu, S.B., Zhao, J.L., 2017b. Crust-mantle interaction during early Jurassic subduction of Neo-Tethyan oceanic slab: evidence from the Dongga gabbro-granite complex in the southern Lhasa subterrane, Tibet. Lithos 292–293, 262–277.

Weller, O.M., St-Onge, M.R., Searle, M.P., Waters, D.J., Rayner, N., Chen, S., Chung, S.L., Palin, R.M., 2015. Quantifying the *P–T–t* conditions of north-south Lhasa terrane accretion: new insight into the pre-Himalayan architecture of the Tibetan plateau. J. Metam. Geol. 33, 91–113.

Xu, B., Hou, Z.Q., Zheng, Y.C., Wang, R., He, M.Y., Zhou, L.M., Wang, Z.X., He, W.Y., Zhou, Y., Yang, Y., 2017a. In situ elemental and isotopic study of diorite intrusions: implication for Jurassic arc magmatism and porphyry Cu-Au mineralization in southern Tibet. Ore Geol. Rev. 90, 1063–1077.

Xu, B., Hou, Z.Q., Zheng, Y.C., Zhou, Y., Zhou, L.M., Yang, Y., Han, Y.W., Zhen, G., Wu, C.D., 2017b. Jurassic Hornblende Gabbros in Dongga, Eastern Gangdese, Tibet: partial melting of mantle wedge and implications for crustal growth. Acta Geol. Sin. 91, 545–564.

Xu, W., Zhu, D.C., Wang, Q., Weinberg, R.F., Wang, R., Li, S.M., Zhang, L.L., Zhao, Z.D., 2019. Constructing the Early Mesozoic gangdese crust in southern Tibet by hornblende-dominated magmatic differentiation. J. Petrol. https://doi.org/10.1093/petrology/egz005.

Yang, Z.M., Hou, Z.Q., Xia, D.X., Song, Y.C., Li, Z., 2008. Relationship between western porphyry and mineralization in Qulong copper deposit of Tibet and its enlightenment to further exploration. Miner. Depos. 27, 28–36 (in Chinese with English abstract).

Yang, J.S., Xu, Z.Q., Li, Z.L., Xu, X.Z., Li, T.F., Ren, Y.F., Li, H.Q., Chen, S.Y., Robinson, P.T., 2009. Discovery of an eclogite belt in the Lhasa block, Tibet: a new border for Paleo-Tethys? J. Asian Earth Sci. 34, 76–89.

Yang, Z.M., Hou, Z.Q., Jiang, Y.F., Zhang, H.R., Song, Y.C., 2011. Sr-Nd-Pb and zircon Hf isotopic constraints on petrogenesis of the Late Jurassic granitic porphyry at Qulong, Tibet. Acta Petrol. Sin. 27, 2003–2010 (in Chinese with English abstract).

Yin, A., Harrison, T.M., 2000. Geologic evolution of the Himalayan-Tibetan orogen. Annu. Rev. Earth Planet. Sci. 28, 211–280.

Yu, Y.P., Xie, C.M., Fan, J.J., Wang, M., Dong, Y.C., Wang, B., Hao, Y.J., 2018. Zircon U–Pb geochronology and geochemistry of Early Jurassic granodiorites in Sumdo area, Tibet: constraints on petrogenesis and the evolution of the Neo-Tethyan Ocean. Lithos 320–321, 134–143.

Zeng, L.S., Liu, J., Gao, L.E., Chen, F.Y., Xie, K.J., 2009. Early Mesozoic high-pressure metamorphism within the Lhasa block, Tibet and implications for regional tectonics. Earth Sci. Front. 16, 140–151.

Zhang, H.F., Xu, W.C., Guo, J.Q., Zong, K.Q., Cai, H.M., Yuan, H.L., 2007a. Indosinian orogenesis of the gangdise terrane: evidences from zircon U-Pb dating and petrogenesis of granitoids. Earth Sci. J. China Univ. Geosci. 32, 155–166 (in Chinese with English abstract).

Zhang, H.F., Xu, W.C., Guo, J.Q., Zong, K.Q., Cai, H.M., Yuan, H.L., 2007b. Zircon U-Pb and Hf isotopic composition of deformed granite in the southern margin of the Gangdese belt, Tibet: evidence for early Jurassic subduction of Neo-Tethyan oceanic slab. Acta Petrol. Sin. 23, 1347–1353 (in Chinese with English abstract).

Zhang, Z.M., Dong, X., Liu, F., Lin, Y.H., Yan, R., He, Z.Y., Santosh, M., 2012. The making of Gondwana: discovery of 650 Ma HP granulites from the North Lhasa, Tibet. Precambrian Res. 212–213, 107–116.

Zhu, D.C., Pan, G.T., Chung, S.L., Liao, Z.L., Wang, L.Q., Li, G.M., 2008. SHRIMP zircon age and geochemical constraints on the origin of Lower Jurassic volcanic rocks from the Yeba Formation, southern Gangdese, South Tibet. Int. Geol. Rev. 50, 442–471.

Zhu, D.C., Mo, X.X., Niu, Y., Zhao, Z.D., Wang, L.Q., Pan, G.T., Wu, F.Y., 2009. Zircon U-Pb dating and in-situ Hf isotopic analysis of Permian peraluminous granite in the Lhasa terrane, southern Tibet: implications for Permian collisional orogeny and paleogeography. Tectonophysics 469, 48–60.

Zhu, D.C., Zhao, Z.D., Niu, Y.L., Mo, X.X., Chung, S.L., Hou, Z.Q., Wang, L.Q., Wu, F.Y., 2011. The Lhasa Terrane: record of a microcontinent and its histories of drift and growth. Earth Planet. Sci. Lett. 301, 241–255.

Zhu, D.C., Zhao, Z.D., Niu, Y.L., Dilek, Y., Wang, Q., Ji, W.H., Dong, G.C., Sui, Q.L., Liu, Y.S., Yuan, H.L., Mo, X.X., 2012. Cambrian bimodal volcanism in the Lhasa Terrane, southern Tibet: record of an early Paleozoic Andean-type magmatic arc in the Australian proto-Tethyan margin. Chem. Geol. 328, 290–308.

Zhu, D.C., Zhao, Z.D., Niu, Y.L., Dilek, Y., Hou, Z.Q., Mo, X.X., 2013. The origin and pre-Cenozoic evolution of the Tibetan Plateau. Gondw. Res. 23, 1429–1454.

Zhu, D.C., Wang, Q., Zhao, Z.D., Chung, S.L., Cawood, P.A., Niu, Y.L., Liu, S.A., Wu, F.Y., Mo, X.X., 2015. Magmatic record of India–Asia collision. Sci. Rep. 5, 14289.

Zou, Y.Q., Huang, W.T., Liang, H.Y., Wu, J., Lin, S.P., Wang, X.Z., 2015. Identification of porphyry genetically associated with mineralization and its zircon U-Pb and biotite Ar-Ar age of the Xiongcun Cu-Au deposit, Southern Gangdese, Tibet. Acta Petrol. Sin. 31, 2053–2062 (in Chinese with English abstract).